Journal of Structural Geology 33 (2011) 381–398

Contents lists available at ScienceDirect

Journal of Structural Geology

journal homepage: www.elsevier.com/locate/jsg

Prograde lawsonite during the flow of continental crust in the Alpine subduction: Strain vs. metamorphism partitioning, a field-analysis approach to infer tectonometamorphic evolutions (Sesia-Lanzo Zone, Western Italian Alps)

Michele Zucali [a,*], Maria Iole Spalla [a,b]

[a] Dipartimento di Scienze della Terra "Ardito Desio", Università degli Studi di Milano, Via Mangiagalli 34, I-20133 Milano, Italy
[b] CNR – Istituto per la Dinamica dei Processi Ambientali, Via Mangiagalli 34, I-20133 Milano, Italy

ARTICLE INFO

Article history:
Received 19 April 2010
Received in revised form
26 October 2010
Accepted 5 December 2010
Available online 17 December 2010

Keywords:
Sesia-Lanzo Zone
Subduction
Lawsonite
Prograde
Strain partitioning

ABSTRACT

Detailed mapping of superposed fabrics and their mineral support allows for reconstruction of the tectonometamorphic evolution of the Ivozio Complex, within the inner portion of the Sesia-Lanzo Zone (Western Italian Alps). The resulting evolution is characterized by a multi-stage structural and metamorphic re-equilibration during Alpine subduction, starting from the pre-Alpine igneous association ($Amp_0 + Cpx_0$). The prograde associations begin with S_{1a} marked by $Amp_I + Zo_I$ which pre-date the growth of Grt_I (S_{1b}); successive increase in pressure stabilizes a second generation of Amp + Grt (S_{1c} Amp_{II} + ZoI + Grt_{II}). The growth of prograde lawsonite and omphacite occur during S_{1d} (Omp_I + Lws + Grt_{II} + Amp_{II}) within **lawsonite-bearing** eclogites, while S_{1e} is associated with the break-down of lawsonite, producing the association Omp_I + Ky + Zo_{II} + Grt_{II} + Amp_{II} (**lws-bearing** eclogites); $S_{1d\text{-}e}$ stages are associated with Amp_{II} + ZoI + Grt_{II} + Omp_I in eclogites. The second generation of penetrative foliation (S_2), describing the retrograde evolution, is divided into S_{2a} (Amp_{II} + GrtII + Pg + Zo_{II}) and S_{2b} (Chl + AmpIII + Pg + Ab). The comparison between the reconstructed evolution of the Ivozio Complex and P–T paths inferred in the Southern Sesia-Lanzo Zone suggests a non-uniqueness of the Sesia-Lanzo Zone continental crust, during the Alpine subduction.

1. Introduction

In order to discriminate between mechanisms active during the subduction burial and exhumation of continental crust (e.g. tectonic erosion, ablative subduction), it is fundamental to determine the Pressure–Temperature–relative time of deformation trajectories followed by the rocks within the subduction wedge. Moreover, the actual dimension and shape of the slices of crust acting as independent object within the subduction system are also crucial. Pressure and temperature variations in time, deduced from numerical modelling and their comparison with thermobarometric and geochronological natural data, suggest that crustal particles, involved in the subduction–collision lithosphere-scale processes, may be recycled within the subduction wedge prior to the exhumation and final, stable structural packaging (Gerya et al., 2002; Meda et al., 2010; Roda et al., 2010).

The occurrence of lawsonite-bearing rocks is the marker of a highly depressed geothermal gradient characterizing the thermal state of very cold subduction zones (Cloos, 1982, 1993). Therefore, discrimination between prograde and retrograde lawsonite within subducted rocks is also crucial to individuate the highly depressed geothermal gradient active during burial and/or exhumation paths. Generally, lawsonite develops within the subducting oceanic lithosphere under extreme LT–HP conditions (Tsujimori et al., 2006; Cetinkaplan et al., 2008; Ghent et al., 2009), while it is rarely reported in continental crust (Sesia-Lanzo Zone – Italy: Compagnoni et al., 1977; Pognante, 1989b; Zucali et al., 2004; Dabie – China: Li et al., 2004; Calabria - Southern Italy: Piccarreta, 1981; Turkey: Okay, 2002; Okay and Whitney, 2010). Therefore, the last occurrence implies that mechanisms promoting the subduction of crustal slices from the overriding continental plate, before continental collision, may be active.

The Sesia-Lanzo Zone of the Western Italian Alps is a continental crust fragment (100 × 10 km-sized) involved in the Alpine subduction and collision. It extensively recorded eclogite-facies low-temperature assemblages in the internal parts, known as the Eclogitic Micaschists Complex. Lawsonite-bearing assemblages were also found in the Sesia-Lanzo Zone eclogites and were mainly interpreted as retrograde (in the EMC: Caron and Saliot, 1969; Compagnoni et al., 1977; Pognante et al., 1980, 1988; Spalla and

* Corresponding author. Tel.: +39 02 50315547.
E-mail address: michele.zucali@unimi.it (M. Zucali).

0191-8141/$ – see front matter © 2010 Elsevier Ltd. All rights reserved.
doi:10.1016/j.jsg.2010.12.006

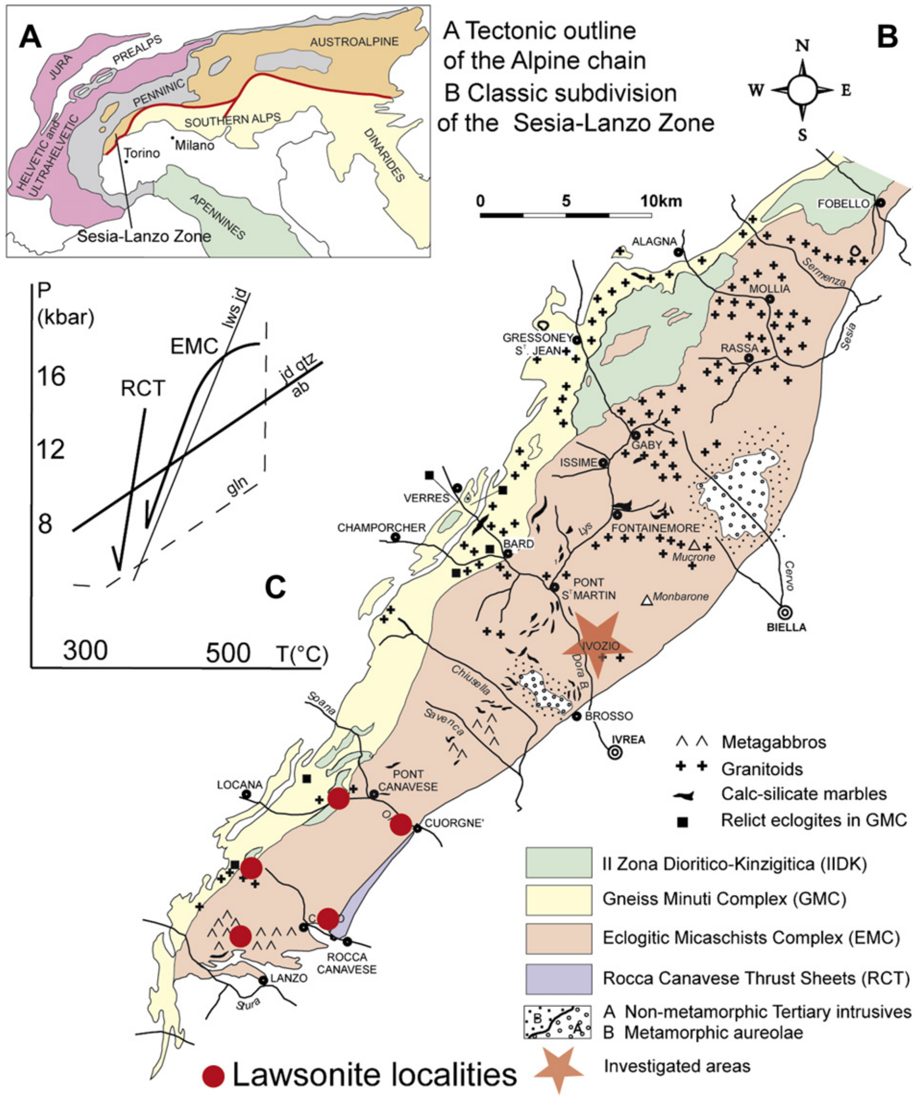

Fig. 1. Tectonic outline of the Alpine chain (A), classical subdivision of the Sesia-Lanzo Zone (B). Pressure–Temperature paths of the lawsonite-bearing rocks from the Rocca Canavese Thrust Sheet (RCT) and Eclogitic Micaschists Complex (EMC) are after Pognante (1989a).

Zulbati, 2003; Zucali et al., 2004; in the IIDK: Miletto, 1984; in the Gneiss Minuti: Pognante et al., 1987).

The use of P–T–d–t paths, supported by detailed regional scale field mapping, has been successfully applied to contour tectonic units with a coherent metamorphic evolution during a time interval (i.e. the tectonometamorphic units, Spalla et al., 2005). Thus, the discrimination of prograde or retrograde lawsonite assemblages is fundamental to individuate contrasted P–T–d–t paths characterizing different tectonometamorphic units in the Sesia-Lanzo Zone.

Strain partitioning and mineral transformation occurring during a multiphase tectonometamorphic evolution may generate different fabrics, partially and/or completely underlined by newly grown minerals or mineral assemblages. These fabrics may be distinguished on the basis of the strain state: low strain (coronitic fabric domains), intermediate strain (tectonitic fabric domains) and high strain (mylonitic fabric domains) (Lardeaux and Spalla, 1990; Spalla and Zucali, 2004). Coronitic fabrics may contain structural and metamorphic mineral relics, allowing for preservation of earlier metamorphic assemblages. In tectonitic and mylonitic fabrics, the metamorphic growth sequence may be linked to the superimposed planar/linear fabrics. Mylonitic fabrics may represent the end-members of both structural and mineralogical re-equilibration, where all mineral and structural relics of pre-existing stages are completely erased. The grain size scale model of deformation partitioning (Bell et al., 1986) enables granular scale deformation stages to be related to successive kinematic stages, from crenulation to complete obliteration of the original fabric (Bell and Rubenach, 1983; Bell and Hayward, 1991; Salvi et al., 2010). The kinematic stages can be related to the evolution of reaction products of metamorphic transformations, distinguishing between fabrics dominantly supported by old minerals, slightly replaced by new minerals (coronitic microstructure of the fabric), and fabrics entirely marked by the new metamorphic assemblages (S or S/L-tectonite to mylonite).

The field-analysis and microstructural correlation of progressive strain states (coronitic, tectonitic and mylonitic fabrics) and the related reacting volumes are here used as the basis of correlation for the tectonometamorphic history (Spalla et al., 1999, 2000; Gazzola et al., 2000; Zucali et al., 2002b; Hobbs et al., 2010; Salvi et al., 2010).

In this contribution, this approach will be applied in order to decipher the tectonometamorphic evolution of the metabasites of the Ivozio Complex. The results will be compared with other

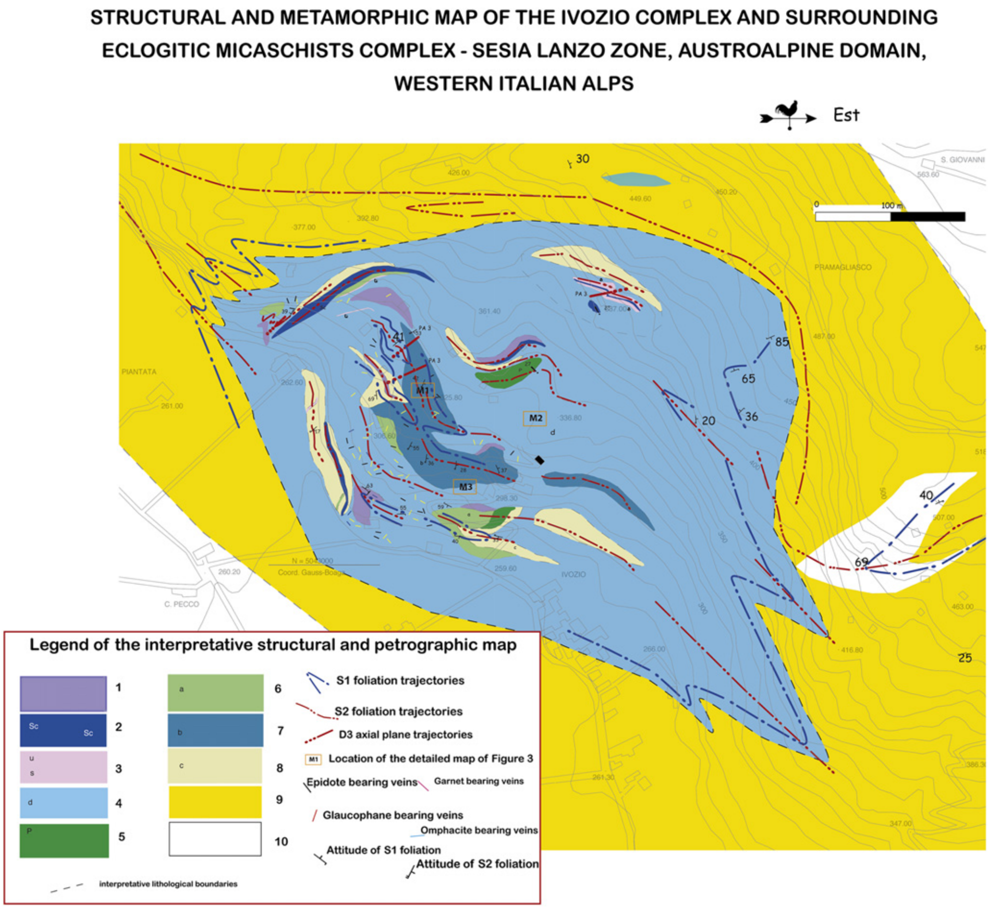

Fig. 2. 1) Eclogitic metabasites: amphibole (40–80%), garnet (10–20%) and minor white mica, epidote and omphacite. The penetrative S2 foliation is marked by the shape preferred orientation of amphibole. Locally relic black-amphibole is wrapped by the main foliation, while large omphacite porphyroblasts overgrow it. 2) Schists: amphibole (20–30%), white mica (40–50%), quartz (20%) and chlorite (≤10%). The penetrative foliation S2 is defined by shape preferred orientation of white mica and amphibole. 3) Ultramafites (u): amphibole (30–40%), white mica (10–20%), chlorite (10%), diopside (≤5%), talc (10%) and minor carbonates and serpentine. The penetrative foliation is marked by alternate amphibole–clinopyroxene and chlorite-talc rich millimetre-size layers. Serpentinites (s): serpentine (≤80%), chlorite, opaques (≤10%), amphibole and pyroxene (≤10%). The foliation (S2) is marked by serpentine rich domains (up to 1-cm-thick) and minor opaque trails. In places serpentinites are associated to carbonate-rich rocks. 4) Alternate layers of various types of eclogite and eclogitic metabasics; layers are about 10 cm in size and parallel to the S2 foliation. 5) Lenses with centimetre-size amphibole and white mica. 6) Omphacite-garnet eclogite: omphacite (40–60%), garnet (30–40%) and minor epidote, white mica and amphibole (≤5%). Granoblastic to foliated fabric with S2 defined by SPO of omphacite. 7) Lawsonite-eclogite: omphacite (20–40%), garnet (5–15%), ex-lawsonite site (2–10%), epidote (10–20%), amphibole (5–10%) and minor paragonite (pseudomorph on lawsonite). This rock is dominated by well developed S1 and S2 tectonitic foliations underlined by the SPO of omphacite, amphibole, paragonite; ex-lawsonite, omphacite and garnet centimetre-size porphyroblasts lay at an angle with respect to S1 and in place show an internal foliation defined by amphibole. 8) Amphibole eclogite: omphacite (40–60%), garnet (20–30%) and amphibole (up to 30%) and minor epidote (locally defining mm-sized layers) and white mica. It is characterized by granoblastic to foliated fabric; in the latter case S2 is the penetrative foliation marked by SPO of omphacite, epidote and amphibole. 9) Omphacite-, glaucophane-, garnet-bearing micaschists. The S1 and S2 foliations are defined by the SPO of phengitic mica, omphacite, glaucophane and quartz. 10) Omphacite-bearing orthogneisses. The S1 foliation is marked by the SPO of phengitic mica, quartz and omphacite.

localities of the Sesia-Lanzo Zone where lawsonite-bearing eclogites were described and a geodynamic environment will be proposed.

2. Geological setting

The Ivozio Complex (Pognante et al., 1980; Zucali et al., 2004) is a part of the Eclogitic Micaschists Complex of the Sesia-Lanzo Zone. The Sesia-Lanzo Zone (Fig. 1) consists of two elements (Dal Piaz et al., 1972; Compagnoni et al., 1977): i) the upper element, "the II Zona Diorito-Kinzigitica" (IIDK), comprises metapelites and metabasites characterized by a dominant pre-Alpine metamorphic imprint under amphibolite/granulite facies conditions; ii) the lower element, consisting of metapelites, metagranitoids, and metabasites, is further divided into two metamorphic complexes: the "Gneiss Minuti Complex" (GMC), showing a dominant Alpine metamorphic imprint under greenschist facies conditions, and the "Eclogitic Micaschists Complex" (EMC), showing a dominant Alpine imprint under eclogite-facies conditions. The pre-Alpine evolution of the Sesia-Lanzo Zone is characterized by a granulite facies stage followed by successive re-equilibrations under amphibolite facies conditions (e.g. Lardeaux and Spalla, 1991). Associated with granulite to amphibolite facies metamorphic stages are metaintrusives (e.g. Ivozio, Monte Mucrone, Lago della Vecchia) of different chemical compositions (felsic and mafic) and ages which occur along the SLZ (Fig. 1) (Compagnoni and Maffeo, 1973; Koons, 1982; Reddy et al., 1996; Rebay and Spalla, 2001; Zucali et al., 2002b). The Alpine evolution is characterized by the polyphase deformation under blueschist to eclogite-facies conditions followed by the retrogression under blueschist to successive greenschist facies conditions (Dal Piaz et al., 1972; Compagnoni, 1977; Compagnoni et al., 1977; Gosso, 1977; Pognante et al., 1980; Zucali et al., 2002b).

P–T estimates for the pre-Alpine evolution show a granulite facies stage in a pressure interval between 0.6 and 0.9 GPa at $T = 700–900$ °C, followed by an amphibolite facies stage defined by $P = 0.3–0.5$ GPa and $T = 570–670$ °C and a greenschist facies re-equilibration at $P = 0.25–0.35$ GPa and $T < 550$ °C (Lardeaux and Spalla, 1991; Rebay and Spalla, 2001). Geochronological estimates and field relationships attribute an age of <270 Ma to the granulite facies stage, an age of <240 Ma to the amphibolite facies, and an age of <170 Ma to the greenschist facies metamorphism. The Alpine eclogite-facies evolution (Koons, 1982; Castelli, 1991; Tropper et al., 1999; Tropper and Essene, 2002; Zucali et al., 2002b) ranges between 60 and 70 Ma (Reddy et al., 1996; Rubatto et al., 1999).

The Ivozio Complex includes eclogitic metabasites, eclogites, lawsonite-eclogites and scarce ultramafics that consist of layers of metapyroxenites and antigorite-serpentinites; primary magmatic layering has also been observed (Pognante et al., 1980; Zucali et al., 2004). The rock-types of the Ivozio Complex have been mutually folded during eclogite to blueschists facies deformation phases, while greenschist facies deformation refolds the main contact between the Ivozio Complex and the surrounding paraschists-metagranitoids of the EMC (B3 deformation phase in Pognante et al., 1980; Zucali et al., 2004). The Alpine metamorphic imprint is penetrative, whereas the pre-Alpine assemblages are scarce. The metabasic protoliths of the Ivozio Complex have been dated by Rubatto (1998) at 355 ± 9 Ma.

3. Mesostructural evolution

The structural–geological map (Fig. 2) shows the field relations of mesostructures occurring in the Ivozio Complex and surrounding EMC. Details of the superimposed structures and mineral growth are in Figs. 3 and 4. Mineral abbreviations are after Kretz (1994) except for amphibole (Amp) and white mica (Wm).

The Ivozio Complex country rocks, mainly record the S_2 foliation (Fig. 2) marked by the shape-preferred orientation (SPO) of eclogite-facies minerals such as Phn + Omp + Amp, associated with Qtz and Grt. An older S_1 foliation is preserved within micaschists as millimetre-thick relics in rootless D_2 folds. S_1 is marked by the SPO of Phn + Amp + Omp and is also associated with Grt. Due to the similarity in the mineral support of both S_1 and S_2, they may be distinguished in the field only when superposition occurs. $S_1 + S_2$ foliations also enclose metre- to decametre-sized eclogite boudins characterized by a penetrative foliation marked by the SPO of Omp + Amp. The S_2 foliation is parallel, at kilometre-scale, to the Ivozio Complex boundary (Fig. 2). At map scale, the S_1 foliation is better preserved within low strain domains that lie parallel to the elongation of the Ivozio Complex metabasic mega-boudin (Fig. 2).

S_1 and S_2 foliations generally strike NE–SW with a highly variable dip angle (0–90°); this variability may be explained as the consequence of the close to isoclinal D_2 geometry; S_1 and S_2 foliations are similar in style, geometry, and shape.

Locally, open D_3 folds overprint S_1 and S_2 foliations (Figs. 2 and 4). The sub-vertical D_3 axial plane also gently bends the lithologic boundaries between the Ivozio Complex and the surrounding EMC (Fig. 2).

Eclogites and hornblendites of the Ivozio Complex show a pervasive foliation that keeps a homogeneous orientation in the area, only gently bent at a kilometre-scale. The bending has a vertical axial plane, not associated with the development of a new planar fabric. The mineral support of the pervasive foliation is Amp + Zo ± Omp ± Grt ± Lws ± Pg (Fig. 4c) and is generally at a low angle to the main lithologic boundaries or mineral layering (Fig. 4b). Metre-scale close to isoclinal folding may occur and relict hinges are also preserved within metre-sized domains (Fig. 4d).

Within the Ivozio Complex, the **S_1 foliation** is defined by a centimetre- to metre-thick compositional layering (Fig. 4). The layering is marked by alternating eclogite types and ultramafic and amphibole-bearing schists (Fig. 2). The SPO of Amp ± mica-rich layers and Zo-rich layers also marks S_1 as parallel to the

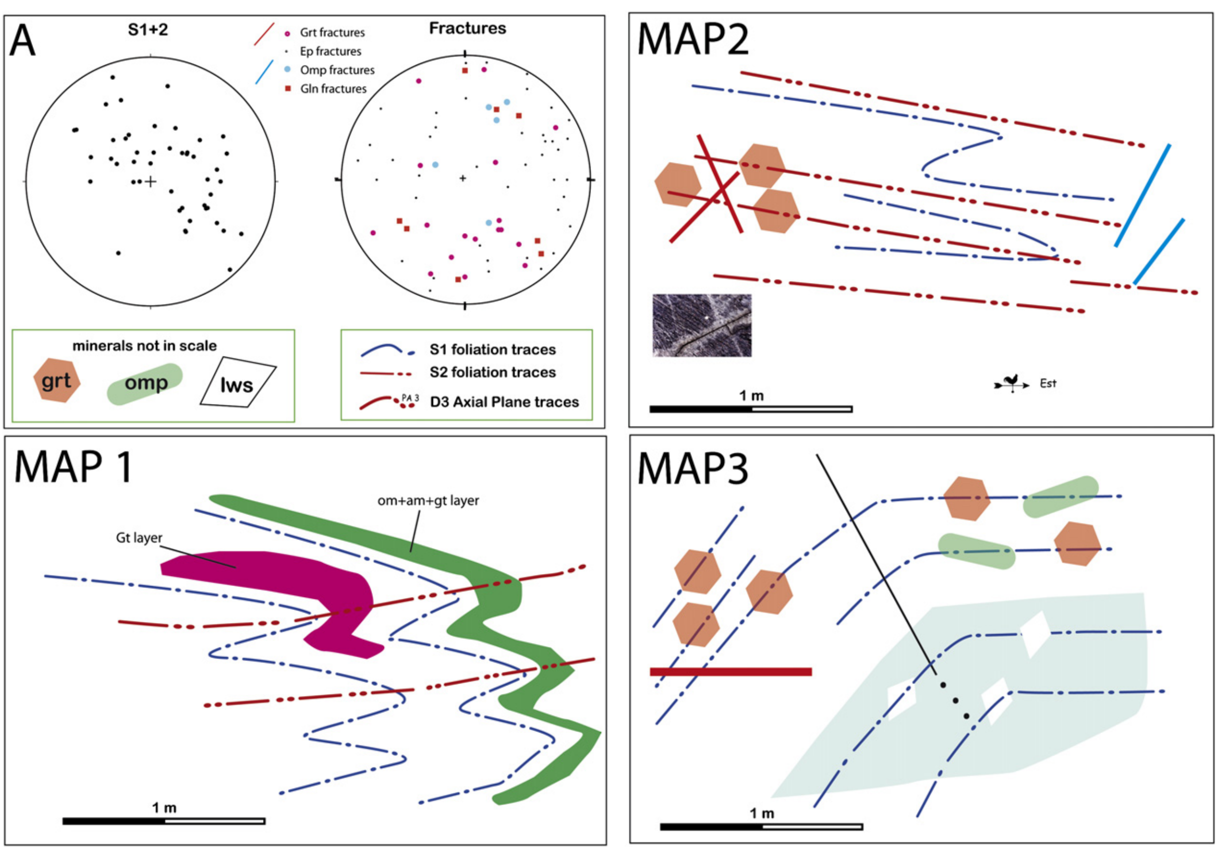

Fig. 3. A) Equal area, lower hemisphere plots of S_{1+2} foliations and fractures. Detailed field geometrical relationships between superimposed fabric elements and minerals are shown in Maps 1, 2, 3. Locations are shown on the map in Fig. 2.


A
B
S0
S1
Lws+Omp
C
D
S1
D2
E
F
G
H
I
L

compositional layering. Mineral layering may be interpreted as primary magmatic layering (**pre-S_1**) only where S_1 intersects decimetre-thick layers of amphibole-bearing eclogites and hornblendites (Fig. 4b).

D_2 folds occur at metre- to decametre-scale (Figs. 2, 3 and 4). D_2 folds are close to isoclinal in shape and bend primary layering and S_1 (Fig. 4d). Metre- to decametre-thick bodies of eclogite are folded and S_2 foliation occurs as an axial planar foliation. S_2 is defined by a millimetre- to centimetre-sized differentiated layering, mainly underlined by the SPO of Amp, Ep, ±Omp, ±Wm, and ±Chl in eclogites (Fig. 4h), hornblendites and schists. S_2 is defined by differentiated layers of Srp and Srp ± Amp in serpentinites and ultramafites. D_2 rootless folds are centimetre-sized relics, better preserved in Amp-schists and eclogites. In eclogites up to centimetre-sized omphacites define a mineral lineation within S_2. In syn-D_2 low strain volumes of eclogites, randomly oriented centimetre-sized omphacite, lawsonite and garnet grains overgrow S_1 underlined by the SPO of Amp + Czo/Zo (Fig. 4c, g). An internal S_1 foliation, marked by Amp ± Wm, occurs within centimetre-sized omphacite and garnet porphyroblasts.

Widespread fracturing occurs within metabasics of the Ivozio Complex. Fractures are filled by omphacite, glaucophane, epidote and garnet (Figs. 3 and 4).

Omphacite veins cut the S_1 foliation (Fig. 4i); close to the omphacite-bearing factures (up to 20 cm) amphiboles of the S_1 foliation are replaced by mimetic or randomly oriented new omphacite grains (Figs. 3 and 4). These newly formed omphacites may also be rimmed by aggregates of glaucophane. The Omp veins' dip azimuth ranges 15–50° towards SW, SE, and NW (Fig. 3).

Glaucophane veins display three principal orientations at about 30° (Fig. 2). They crosscut S_1 and S_2. Glaucophane occurring within these veins may also be rimmed by omphacite. These observations lead to the interpretation that glaucophane veins occurred pre and post to the omphacite-bearing veins. The Gln veins' dip azimuth varies among SW, NW and NE with dip angles between 45 and 70° (Fig. 3).

Epidote veins are characterized by fibrous growth perpendicular to the vein wall. Epidote may also display rims of Gln or Omp. Epidote veins may be up to 3 cm in size (Fig. 4l) and show a random distribution (Fig. 3).

Garnet veins are generally massive and up to 1 m in length. Two orientations may be recognized, generally forming an angle of about 30°; the first group has its dip azimuth at SSW or NNE with dip angles from 70 to 90°, while the second has a lower dip azimuth (0–45°) mostly towards N (Fig. 3). Grt veins may display an Omp-rich rim, suggesting a stage of Omp + Grt veining.

4. Microstructural history and associated micro-chemical evolution

Microstructural analysis was aimed at defining the deformation–metamorphism relationships. Fig. 5 schematically shows the relationships between microstructural evolution and mineral growth derived from microstructural analysis reported in the following paragraphs.

The record of the multi-stage deformation history detected at the meso-scale is more completely recorded in eclogites, which will be therefore described here. For the microstructural characters of micaschists, ultramafics, and hornblendites the reader is addressed to Zucali et al. (2004). Chemical compositions of mineral phases occupying different microstructural positions are described together with the microstructural evolution. Minerals were analysed with an electron microprobe (EMPA – JEOL 8200 Super Probe) and a scanning electron microscope (SEM – Cambridge Stereoscan 360 ISIS 300 Oxford) (Dipartimento di Scienze della Terra "A. Desio" – Università degli Studi di Milano). The operating conditions were 20 kV accelerating voltage, filament intensity of 1.70 A and probe intensity of 280 pA for EMPA and 15 kV accelerating voltage and sample current of 190 pA for SEM. Natural silicates were used as standards; matrix corrections were calculated with the ZAF procedure. Representative mineral compositions are shown in Table 2.

The microstructural evolution is characterized by the development of the two main foliations S_1 and S_2 and by successive stages of mineral growth (Fig. 5). Different stages of mineral growth and foliation development have been recognized at the microscale; on these grounds five stages have been separated in S_1 (S_{1a}–S_{1c}, post-D_{1a} and D_{1b}) and two in S_2 (S_{2a} and S_{2b}).

4.1. Pre-Alpine evolution

Amp-bearing eclogites preserve brownish Rt-rich Amp_0 and Cpx_0 (Fig. 6a), which do not show any SPO; Amp_0 and Cpx_0 generally occur as relicts rimmed by light blue–green CaNa-amphibole (Amp_I) and epidote (Fig. 5). They have lobate margins and undulose extinction and are wrapped by S_1 or S_2 foliations. These relicts are interpreted as pre-Alpine remnants.

4.2. Alpine evolution

4.2.1. D_1

S_1 foliation is preserved in Amp-bearing eclogites and hornblendites as millimetre-sized foliation marked by the SPO of Amp + Zo ± Wm ± Grt. S_{1a} is included within Grt_I porphyroblasts and is defined by the SPO of Amp_I and Zo_I (Fig. 6b). The SPO of Amp_I + Zo_I marks the S_{1b} foliation together with Grt_I. Amp_I, when included in Grt_I, is characterized by smaller grain size if compared with Amp_I in the matrix.

S_{1c} corresponds to the growth of Grt_{II} rims and Amp_{II} larger crystals (Fig. 6b). Garnets show a progressive compositional variation from Grt_I cores to Grt_{II} rims, mainly marked by an increase in the Mg content, which is in the range 7.8–10.3 a.p.f.u. (Table 1 and Fig. 7). The corresponding Py and Alm molecules vary linearly as in Fig. 7 and Table 1 and Grs content decreases from Grt_I cores to Grt_{II} rims.

The successive static growth of centimetre-sized Lws crystals in association with Grt_{II}, Amp_{II} and Omp_I in Lws-bearing eclogites marks the post-D_{1a} stage (Fig. 6c). Lws microsites preserve the original shape (Fig. 6c), which is neither elongated parallel to the S_1 foliation nor deformed. Lws microsites also show rational boundaries

Fig. 4. A) View of the Ivozio village and Carema vineyards from the Montestrutto hill. B) Centimetric S_0 layering defined by alternate bending with different mineral composition. S_1 is marked by mm-sized foliation underlined by the SPO of epidote and omphacite overgrown by millimetre lawsonite crystals. The angular relationships between S_0 and S_1 are also shown. C) Close-up of lawsonite crystals. Characteristic is their light blue colour due to the complete replacement by kyanite + epidote. D) Alternate compositional layering parallel to the S_1 foliation folded during D_2 deformational phase. Light layers are mainly constituted by epidote, white mica, amphibole and omphacite while darker layers are garnet-bearing hornblendites. E) Lawsonite-bearing eclogites with cm-sized garnet crystals alternated with garnet-bearing eclogites characterized by folded cm-thick garnet-rich layers. F) Close-up of garnet-bearing hornblendites. Cm-sized porphyroblastic garnets show an internal foliation marked by the shape preferred orientation of amphibole and epidote (S_1). G) Lawsonite-bearing eclogites with cm-sized crystals randomly grown over the S1 foliation marked by SPO of omphacite and epidote. H) S2 foliation marked by thin white layers of paragonitic-mica and epidote alternate to greenish layers of omphacite. Cm-sized garnet porphyroblasts also occur. I) Omphacite-bearing vein crosscuts S_1 foliation defined by amphibole and omphacite in association with garnet. L) Epidote-bearing vein crosscuts S_1 foliation marked by the SPO of epidote and amphibole associated with mm- to 1 cm-sized garnets. (For interpretation of the references to colour in this figure legend, the reader is referred to the web version of this article).

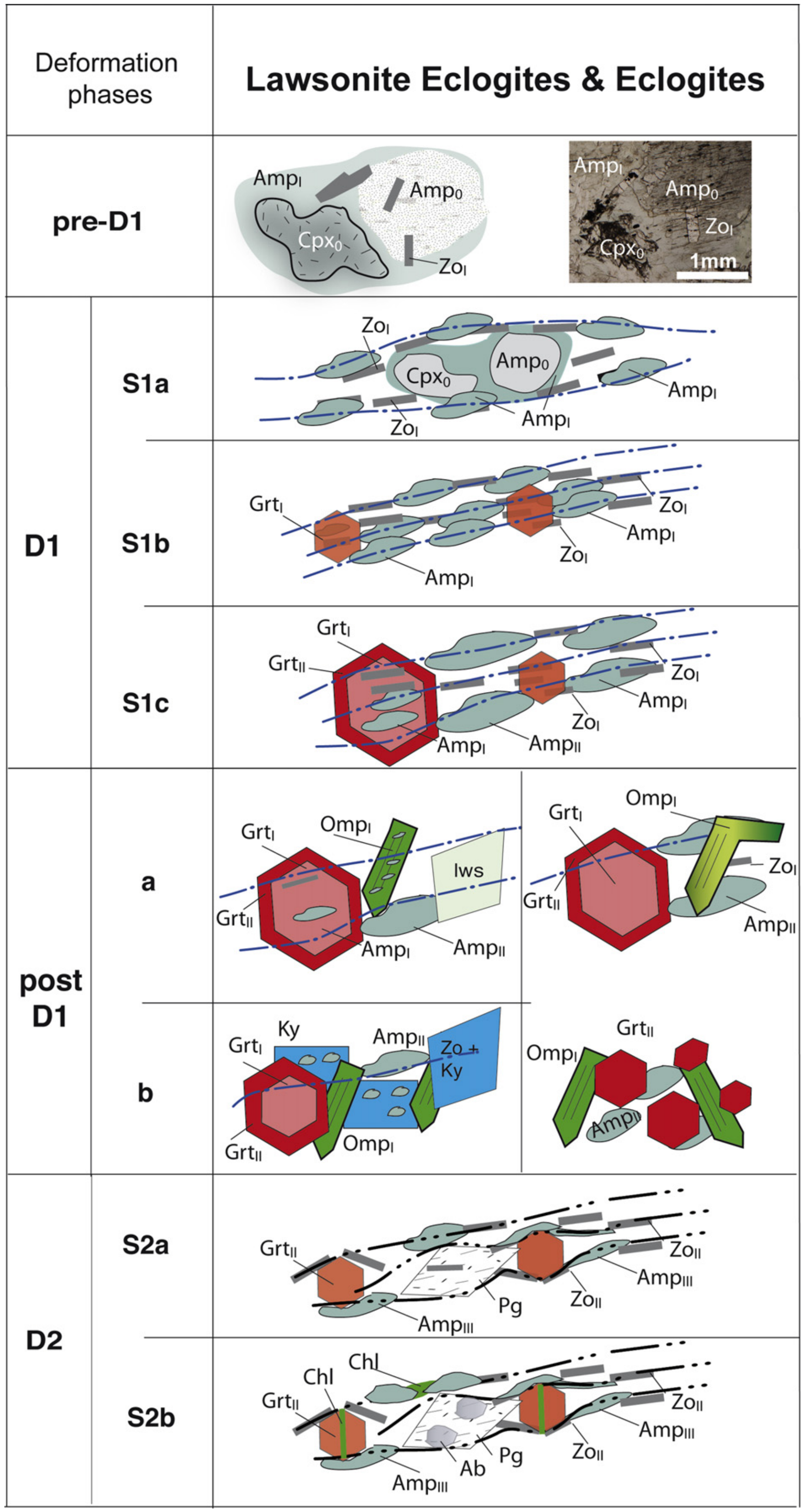

Fig. 5. Schematic view of the microstructural relationships inferred from microstructural analysis for lawsonite-bearing eclogites and eclogites.

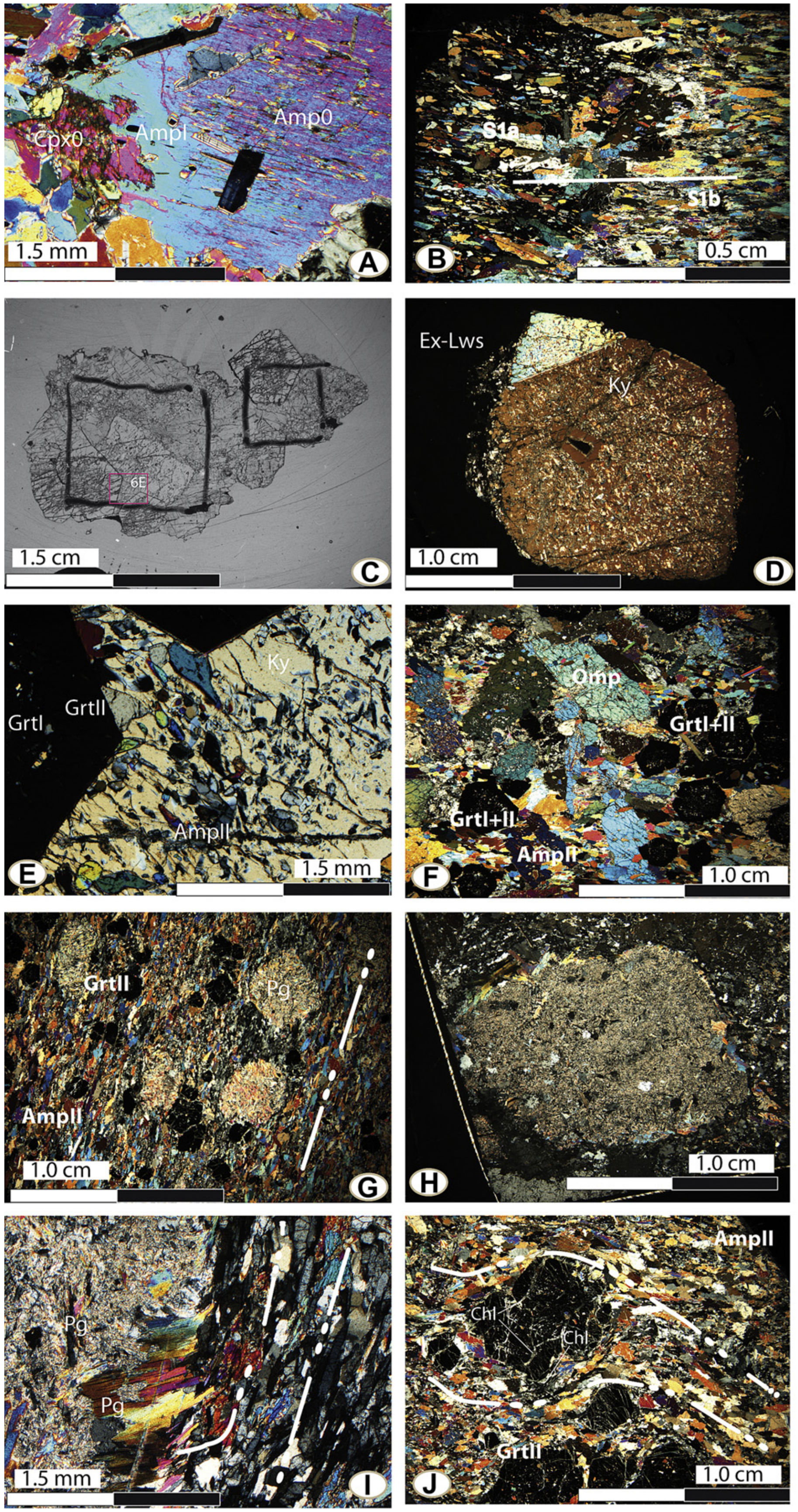
Cpx0
AmpI
Amp0
1.5 mm
A
S1a
S1b
0.5 cm
B
6E
1.5 cm
C
Ex-Lws
Ky
1.0 cm
D
Ky
GrtI
GrtII
AmpII
1.5 mm
E
Omp
GrtI+II
GrtI+II
AmpII
1.0 cm
F
GrtII
Pg
AmpII
1.0 cm
G
1.0 cm
H
Pg
Pg
1.5 mm
I
AmpII
Chl
Chl
GrtII
1.0 cm
J

with Grt_{II} and Omp_I. Omp_I millimetre- to centimetre-sized crystals include Amp_{II} and Zo_I.

Post-D_{1b} is characterized by the growth of millimetre- to centimetre-sized Ky, Omp and Grt_{II} crystals, associated with the destabilization of Lws. Ex-Lws micro-domains (Fig. 6d) are replaced by large Ky crystals with inclusions of idiomorphic Zo_{II}. Amp_{II} locally occurs as interstitial grains defining an SPO. Ky porphyroblasts often include fine-grained Omp_{II} and Amp_I.

In bimineralic eclogites the post-$D1_{a-b}$ stages are associated with the growth of large (centimetre-sized) crystals of Omp_I and Grt_{II} that is locally parallel to the S_1 foliation (Fig. 6f). Omp_I is characterized by undulose extinction and several grains, grown at a high angle with S_1, are bent. Amp_{II} occurs in association with Omp_I and Grt_{II} (Fig. 6f). Amp_I and Amp_{II} in Lws-bearing eclogites are homogeneous and show a lower Si content with respect to Amp_{II} in eclogites (Fig. 7). Amp_{II} in eclogites has Si between 7.5 and 7.75 a.p.f.u., Mg# (= Mg/(Mg + Fe)) is extremely homogeneous across different amphiboles in different rocks (Fig. 7 and Table 1). Epidotes marking the S_1 foliation are zoisites with Fe^{3+} content below 0.1 a.p.f.u. (Table 1). Rutile also marks the S_1 foliation.

4.2.2. D_2

D_2 is characterized by the development of a penetrative foliation, mainly underlined by the SPO of Amp_{III}. Amp_{III} shows similar optical characters and chemical composition to Amp_I and Amp_{II}. Amp_{III} + ZoII + Wm are elongated parallel to the S_2 foliation (Figs. 6g–l); the syn-S_2 mineral association comprises also Grt, which is generally wrapped by Amp_{III} and Zo_{II} aggregates (Fig. 6h). The last feature is also used, together with the associated mineral assemblage and compositions, to distinguish between S_{1c} and S_{2a} foliations that are similar from a mineralogical point of view but differ as microstructures: in S_{1c}, Amp_{II} are truncated by Grt_{II} porphyroblasts while in S_{2a}, Amp_{III} deflects around the Grt_{II} porphyroblasts. Lws is replaced by aggregates of Pg-mica and Zo elongated parallel to S_{2a} (Fig. 6). Pg aggregates mainly occur flattened into the S_{2a} foliation or, in lower strain domains, Pg grains are scattered in the pseudomorphs' cores and are oriented at the rims where they asymptotically join the S_{2a} foliation. Paragonite grown as pseudomorphs on lawsonite shows Na/(Na + K) contents higher than 0.93. Fe^{tot} and Mg contents are below 0.04 a.p.f.u. Several Ab grains occur with Pg within ex-Lws sites. Ab does not show any intracrystalline deformation.

S_{2b} occurs as mechanical reactivation of the S_{2a} foliation that also produces fracturing of Grt and Amp. Grt cracks are filled by Chl, whereas Amp_{II} are also boudinaged and blue–green Amp_{III} + Chl fill deformation necks. Ab + Chl + Czo also mark the S_{2b} foliation. During D_3 S_1 and S_2 foliations are folded and aggregates of Chl, blue–green Amp_{III}, Ab, and Ep occur within microfold-hinges. Locally, the SPO of Amp_{III}, Ep and Chl-rich aggregates underline a S_3 axial plane foliation. Amp_{III} and Ab may also occur as coronas around Omp and $Amp_{I/II}$. Rt grains are replaced by Ttn. The mineralogical assemblage marking S_{2b}, Amp_{III} + Chl + Ab + Czo, corresponds to the mineral paragenesis grown during D_3; this allows us to interpret S_{2b} as a reactivation of S_2 during D_3.

The microstructural relations described above allowed us to define the stable parageneses during successive stages of mechanical re-equilibration, and to relate mineral growth to metamorphic reactions as synthesized in Table 1.

5. Pressure and temperature evolution

Fig. 8 reports pressure and temperature estimates obtained using various thermobarometer calibrations and isochemical phase diagrams. Isochemical phase diagrams (or pseudosections) (Ghent et al., 2009) were calculated for eclogites and lawsonite-bearing eclogites model systems, using Perple_X software (Connolly, 1990) and following the procedure outlined by several authors (Connolly, 2005; Tinkham and Ghent, 2005; Caddick and Thompson, 2008). The system used for modelling is Na_2O–CaO–FeO–MgO–Al_2O_3–SiO_2–H_2O. The P–T range is 0.5–3.0 GPa and 200–700 °C. The following solid-solution models have been used: garnet, phengite (Holland and Powell, 1998), omphacite (Green et al., 2007), amphibole (Dale et al., 2000, 2005), chlorite (Holland et al., 1998) and feldspar (Furman and Lindsely, 1988). Holland and Powell's thermodynamic database (2002) was used for the calculations. The eclogite P–T pseudosection has been calculated using the bulk composition reported by Rubatto (1998) for eclogite of the Ivozio Complex (Fig. 8a). The P–T pseudosection for lawsonite-bearing eclogite has been calculated using the bulk composition obtained by combining mineral modes from thin section analysis with corresponding electron microprobe analyses, considering minerals occurring in the post-D_{1a} assemblage. Rock compositions are given in Fig. 8. In the calculations we assume that: i) H_2O was in excess and was the only fluid phase and ii) SiO_2 was saturated in the systems.

The two calculated pseudosections describe the typical phase relations described for various basic systems (Poli and Schmidt, 1995; Ballevre et al., 2003; Clarke et al., 2006; Rebay et al., 2010). Lws-consuming reactions comprise Lws + Am = Zo + Pg + Grt + Qtz + H_2O, Lws + Cpx = Pg + Zo + Qtz + H_2O, Lws + Grt = Zo + Grt + H_2O, Lws = Zo + Pg + Qtz/Coe + H_2O, and Lws = Zo + Ky + Qtz/Coe + H_2O (Poli and Schmidt, 1995; Okamoto and Maruyama, 1999). Mineral assemblages predicted by pseudosections are coherent with the sequence of mineral growth with respect to deformation as inferred by microstructural analysis (Fig. 5 and Table 1). In the following, peculiar mineral assemblages variation referred to each stage of fabric evolution will be described.

Pre-D_1: no P–T constraints are available for this stage because the original chemical compositions of Cpx and Amp are completely re-equilibrated during Alpine metamorphism.

S_{1a}: pseudosection in Fig. 8a shows the stability field of the assemblage Chl + Amp + Zo + Qtz + H_2O that defines the S_{1a} fabric development in a pressures range of 0.5–1.3 GPa for temperatures of 300–500 °C (Fig. 8a).

$S_{1b\text{-}c}$: Amp_I + ZoI + Grt_I are stable at pressures of 1.15–1.8 GPa and temperatures between 470 and 550 °C (Fig. 8a). Temperatures of 385 ± 12 °C are also constrained by Grt_I–Amp_I exchange for the S_{1b} stage and 530 ± 50 °C (Grt_{II}–Amp_I) for the S_{1c} stage (Ravna, 2000) (Fig. 8a,c).

Fig. 6. A) Low strain domain preserving Amp_0 and Cpx_0 magmatic grains within eclogites. Amp_0 and Cpx_0 are rimmed by Amp_I; individual grains of Zo_I also occur. B) Cm-sized garnet porphyroblast encloses Amp_I aggregates, preserving a well defined SPO (S_{1a}). Garnet porphyroblast rim (Grt_{II}) enclose larger amphibole individuals that define a continuous external foliation (S_{1b}). C) Wide angle view of lawsonite-bearing eclogites where the rhombohedral shape of the ex-lawsonite microsites are well preserved, though completely replaced by Ky + Zo_I aggregates. D) Ex-lawsonite microsite which preserves the rhombohedral shape of the original lawsonite, now pseudomorphosed by the association Ky + Zo. E) Close-up to the grain boundaries between Grt_{II} and Ky crystal pseudomorphs after lawsonite. Grt_{II} define the outer rim of cm-size skeletal Grt_I while Ky individuals enclose numerous Amp_{II} + Zo_{II} grains free of preferred orientations. F) Large Omp individuals at an angle with respect to S_1 (post-$D_{1a\text{-}b}$) with intracrystalline strain (see also Fig. 5) and rich in Amp_I inclusions. Garnet porphyroblasts preserve Grt_I cores rich in Amp_I inclusions but free of Omp. Large Amp_{II} individuals define the S_1 foliation by SPO. G) Rhombohedral ex-lawsonite microsites within the S_2 foliation; ex-lawsonite microsite are replaced by pseudomorphs paragonitic-mica; paragonitic-mica occurs in randomly oriented aggregates (H) or may be gently flattened and oriented parallel to S_2 foliation (I). J) S_{2b} foliation marked by the preferred orientation of Amp_{II} wrapping Grt_{II} porphyroclasts partially fractured and replaced by aggregates of Chl.

Table 1
Stable metamorphic assemblages and metamorphic reactions inferred by microstructural analysis.

Deformation Phase	Stage	Stable assemblage	Metamorphic Reactions	
			eclogite	lawsonite-eclogite
pre-D_1		Cpx0 + Amp0		
D_1	S_{1a}	AmpI + ZoI	Amp0 + Cpx0 + Pl => AmpI + ZoI	
	S_{1b}	AmpI + ZoI + GrtI	AmpI + ZoI => AmpI + ZoI + GrtI	
	S_{1c}	AmpII + ZoI + GrtII	AmpI + ZoI + GrtI => AmpII + ZoI + GrtII	
post-D_1	a	OmpI + Lws + GrtII + AmpII		a) AmpII + ZoI + GrtII => Lws + OmpI + GrtII ± AmpII
	b	OmpI + Ky + ZoII + GrtII + AmpII (lws-bearing eclogites)	AmpII + ZoI + GrtII => OmpI + GrtII + ZoI ± AmpII	b) Lws + OmpI + GrtII ± AmpII => Ky + Zo + OmpI + GrtII ± AmpII
		AmpII + ZoI + GrtII + OmpI (eclogites)		b) Lws = Ky + Zo + H2O
D_2	S_{2a}	AmpII + GrtII + Pg + ZoII		a) Ky + Zo + OmpI + GrtII ± AmpII => AmpII + GrtII + Pg + ZoII;
	S_{2b}	Chl + AmpIII + Pg + Ab	AmpII + GrtII + Pg + ZoII => AmpIII + Ab + Pg + Fe-Ep + Chl	b) Omp + Ky = Amp + Pg + Ep AmpII + GrtII + Pg + ZoII => AmpIII + Ab + Pg + Fe-Ep + Chl
D_3		AmpIII + Chl + Pl + Ep + Ttn ± Grt ± Qtz	Omp + Qtz = Pl + Ep Pg = Ab + H2O Omp + Grt = AmpIII + Grt + Ep Cpx + Rt + Wm = Chl + Ttn + Qtz	Omp + Qtz = Pl + Ep Pg = Ab + H2O Omp + Grt = AmpIII + Grt + Ep Cpx + Rt + Wm = Chl + Ttn + Qtz

Post-D_{1a}: Omp_I + Lws + Grt_{II} + Amp_{II} are stable at pressures above 1.8 GPa for temperatures of 520–600 °C as shown in pseudosection (Fig. 8b). The Lws + Omp = Wm_I (Pg) + Ep reaction, calibrated in basaltic systems, constrains maximal temperature for the Lws stability (Poli and Schmidt, 1998) (Fig. 8c).

Post-D_{1b}: Omp_I + Ky + Zo_{II} + Grt_{II} + Amp_{II} (**lws-bearing** eclogites) assemblage is stable at temperatures >580 °C and at pressures >1.5 GPa, as shown by the calculated assemblage am + g + o + ky + zo in the pseudosection (Fig. 8b). The destabilization of Lws, following the reaction Lws = Zo + Ky + Qtz + H2O (Fig. 8c), refines the constraints at $T > 600$ °C and $P > 2.25$ GPa and Qtz = Coe transition limits the upper pressure at 2.7 GPa.

Post-D_{1a-b}: The Amp_{II} + ZoI + Grt_{II} + Omp_I (eclogites) assemblage is stable for temperatures >550 °C and pressures >1.5 GPa (Fig. 8a). Kd between Grt_{II} and Omp_I (Krogh-Ravna and Terry, 2004) also constraints $P > 1.7$ GPa and $T = 550–650$ °C (Fig. 8c).

S_{2a}: Amp_{II} + GrtII + Pg + Zo_{II} is stable at pressures of 1.15–1.8 GPa and temperatures of 500–600 °C (Fig. 8a–b). These P–T conditions are also constrained by the Lws, Omp and Ky break-down reactions: Lws + Omp = Pg + Zo + Qtz, and Omp + Ky = Amp + Pg + Zo (Fig. 8a–c).

S_{2b}: Chl + AmpIII + Pg + Ab coexistence indicates a pressures range of 0.5–1.3 GPa for temperatures between 300 and 500 °C (Fig. 8).

Assemblages in pseudosections (Fig. 8) well fit the microstructural interpretations that constraint the relative chronology of the assemblages as well as the lawsonite growth during the post-D_{1a} stage, and its disappearance during the retrograde stage post-D_{1b} following the break-down reaction Lws = Zo + Ky + Qtz/Coe + H_2O (Poli and Schmidt, 1995; Okamoto and Maruyama, 1999). S_{1a} to S_{1c} stages within the lawsonite-bearing eclogite have not been constrained, but the prograde stages modelled for the lawsonite-free eclogite (hatched grey line in Fig. 8b) confirm that the growth of lawsonite occurred during the post-D_{1a} stage. Moreover, lawsonite-bearing eclogites do not preserve lawsonite during the retrograde stages because of the increasing temperature path, documented by the post-D_{1a} assemblages (Ballevre et al., 2003; Clarke et al., 2006; Tsujimori et al., 2006; Rebay et al., 2010).

6. Discussion

The P–T–d–t path followed by the Ivozio metabasites is characterized by a multi-stage structural and metamorphic re-equilibration during Alpine time: i) the S_1 foliation developed at evolving P–T conditions from 0.5 to 1.3 GPa at T = 300–500 °C (S_{1a}) to $P < 1.8$ GPa and $T < 600$ °C; ii) post-D_1 stages are characterized by the static growth of lawsonite (post-D_{1a}) and by the subsequent replacement of lawsonite by omphacite + zoisite + kyanite assemblages (post-D_{1b}). Post-D_{1a} occurred at 1.8 GPa and 520–600 °C, while post-D_{1b} is constrained at $P > 1.5$ GPa and at $T > 580$ °C. iii) The subsequent development of the S_2 foliation occurred at decreasing P and T. S_{2a} occurred at $P < 1.8$ GPa and T between 500 and 600 °C, while S_{2b} at P = 0.5–1.3 GPa and T = 300–500 °C.

Prograde stages correspond to a geothermal gradient of ≈10 °C/km (stages S_{1a} to S_{1c}). The peak pressure conditions (post-D_{1a-b}) correspond to a geothermal gradient interval of 6.5–9 °C/km taking into account a minimal pressure of 2.0 GPa at T = 550 °C for the recorded mineralogical assemblages. The retrograde path is marked by a first temperature increase at constant or decreasing pressure, related to a geothermal gradient between 12 and 10 °C/km (stages S_{2a}–S_{2b}).

Table 2
Selected microprobe analysis. Mineral formula has been recalculated using JPT (Zucali, 2009).

Amphibole								
Rock Sample	IV19b_P20_am1	IV19b_P21_am2	IV19b_P18_am2	19bC1 P2	19bC1 P3	IV19b_P30_am2	IV19 C3 P6	IV14a C6 P
Mineral	am	am	am	am	am	am	am	am
SiO_2	51	51.15	50.09	51.95	51.92	51.31	55.87	55.27
TiO_2	0.16	0.38	0.24	0.16	0.14	0.23	0.06	0.05
Al_2O_3	11.46	12.17	11.52	11.44	11.66	11.62	3.41	1.33
FeO	5.06	5.06	5.05	4.91	4.97	4.98	8.86	4.97
MnO	0.08	0.19	0.06	0	0.05	0.01	0.22	0.11
MgO	16.66	16.7	16.37	17.61	17.5	16.72	16.58	22.22
CaO	8.8	8.79	8.9	8.54	8.5	9.03	11.63	12.04
Na_2O	4.57	4.61	4.59	3.4	3.51	4.54	1.25	0.84
K_2O	0.25	0.21	0.31	0.25	0.26	0.16	0.06	0.03
Sum	**98.04**	**99.26**	**97.13**	**98.26**	**98.51**	**98.6**	**97.94**	**96.86**
Ox	23	23	23	23	23	23	23	23
Si	7.081	7.015	7.035	7.141	7.124	7.076	7.841	7.748
Ti	0.017	0.039	0.025	0.017	0.014	0.024	0.006	0.005
Al	1.875	1.967	1.907	1.853	1.885	1.888	0.564	0.22
Fe_2	0.587	0.58	0.593	0.564	0.57	0.574	1.04	0.583
Mn	0.009	0.022	0.007	0	0.006	0.001	0.026	0.013
Mg	3.449	3.415	3.428	3.609	3.58	3.437	3.469	4.644
Ca	1.309	1.292	1.339	1.258	1.249	1.334	1.749	1.808
Na	1.23	1.226	1.25	0.906	0.934	1.214	0.34	0.228
K	0.044	0.037	0.056	0.044	0.046	0.028	0.011	0.005
cationSUM	15.602	15.593	15.639	15.391	15.408	15.577	15.046	15.254
T	8	8	8	8	8	8	8	8
AlIV	0.919	0.985	0.965	0.859	0.876	0.924	0.159	0.252
AlVI	0.956	0.982	0.942	0.994	1.009	0.964	0.405	0
C	5.018	5.038	4.995	5.184	5.179	5	4.946	5.245
(Ca + Na)B	2	2	2	2	2	2	2	2
NaB	0.691	0.708	0.661	0.742	0.751	0.666	0.251	0.192
NaA	0.539	0.518	0.589	0.164	0.183	0.548	0.089	0.036
(Na + K)A	*0.583*	*0.555*	*0.645*	*0.208*	*0.229*	*0.576*	*0.1*	*0.041*
Fe/Mg	0.17	0.17	0.17	0.16	0.16	0.17	0.30	0.13

Omphacite										
Sample	19C3 P3	19bC1 P2	19bC1 P3	19bC1 P4	19bC1 P7	19bC3 P5	19bC3 P6	19bC4 P1	19bC4 P2	19bC3/4 P1
an.	eclo	eclo	eclo	eclo	eclo	eclo	eclo	eclo	eclo	eclo
K_2O	0.25	0.26	0.25	0.24	0.24	0.26	0.24	0.22	0.23	
CaO	14.48	8.54	8.5	8.37	8.61	9.13	8.7	8.79	9.32	8.69
TiO_2	0.11	0.16	0.14	0.21	0.16	0.13	0.4	0.52	0.14	0.25
Cr_2O_3	0	0.01	0.09	0	0.01	0	0.05	0.02	0.01	0.01
MnO	0.02	0	0.05	0.05	0.01	0.01	0.03	0	0.01	0.04
FeOt	2.91	4.91	4.97	4.99	4.93	5.15	4.86	4.91	4.78	5.05
NiO	0	0	0	0	0	0	0	0	0	0
Na_2O	6.51	3.4	3.51	3.55	3.47	3.23	3.75	3.58	3.19	3.88
SiO_2	57.04	51.95	51.92	52.24	52.1	53.65	52.7	52.78	53.56	52
Al_2O_3	10.85	11.44	11.66	11.76	11.38	10.5	11.48	10.87	9.8	12.44
MgO	8.99	17.61	17.5	17.58	17.6	16.05	15.57	16.12	16.57	15.6
TOTAL	100.91	98.27	98.6	99	98.51	98.09	97.8	97.83	97.6	98.19
factor	2.11	2.15	2.15	2.14	2.15	2.15	2.16	2.16	2.16	2.16
(S)	3.99	4.01	4.02	4.02	4.02	3.97	3.99	3.99	3.98	4
formula: 4 cations, 6 oxygens										
Si	2.003	1.856	1.848	1.852	1.856	1.938	1.903	1.905	1.941	1.866
Al.IV	0	0.144	0.152	0.148	0.144	0.062	0.097	0.095	0.059	0.134
Al.VI	0.449	0.337	0.338	0.343	0.334	0.386	0.391	0.368	0.36	0.392
Ti	0.003	0.004	0.004	0.006	0.004	0.004	0.011	0.014	0.004	0.007
Cr	0	0	0.003	0	0	0	0.001	0.001	0	0
Fe^{3+}	0	0.045	0.058	0.049	0.051	0	0	0	0	0.009
Fe^{2+}	0.085	0.102	0.09	0.099	0.096	0.156	0.147	0.148	0.145	0.142
Mg	0.471	0.937	0.928	0.929	0.935	0.864	0.838	0.867	0.895	0.834
Ni	0	0	0	0	0	0	0	0	0	0
Mn	0.001	0	0.002	0.002	0	0	0.001	0	0	0.001
Ca	0.545	0.327	0.324	0.318	0.329	0.353	0.337	0.34	0.362	0.334
Na	0.443	0.235	0.242	0.244	0.24	0.226	0.263	0.251	0.224	0.27
K	0	0.011	0.012	0.011	0.011	0.011	0.012	0.011	0.01	0.011
Σcats	4	4	4	4	4	4	4	4	4	4
FeO	2.91	3.41	3.01	3.33	3.21	5.15	4.86	4.91	4.78	4.74
Fe_2O_3	–	1.67	2.18	1.85	1.91	–	–	–	–	0.35
newTotal	100.91	98.44	98.82	99.19	98.7	98.09	97.8	97.83	97.6	98.22
Jd	0.443	0.247	0.254	0.255	0.251	0.237	0.274	0.262	0.234	0.28

(continued on next page)

Table 2 *(continued).*

Garnet							
Rock sample	iv19bp2_grt1	19C3P7_grt1?	19bC2 P1_grt2	19bC2 P2_grt1	IV19b_P2_grt1	IV19b_P14_grt2	IV19b_P28_grt2
Mineral	gt	gt	gt	gt	gt	gt	gt
SiO_2	38.81	40.709	39.6	39.15	38.6	38	38.95
TiO_2	0	0.039	0.02	0.03	0.08	0.04	0.01
Al_2O_3	22.729	21.599	22.23	22.41	22.24	21.96	22.62
FeO	20.721	21.021	20.13	21.74	22.35	20.7	20.8
MgO	8.668	7.86	10.29	8.59	7.8	10.27	10.36
CaO	7.372	8.438	7.2	7.76	7.63	7.27	7.32
Na_2O	0.038	0.01	0	0	0.72	0.73	0.61
K_2O	0	0.01	0	0	0.08	0	0
Sum	98.338	99.685	99.47	99.68	99.5	98.97	100.67
Ox	12	12	12	12	12	12	12
Si	2.986	3.092	2.979	2.978	2.765	2.561	2.652
Ti	0	0.002	0.001	0.002	0.004	0.002	0.001
Al	2.061	1.933	1.971	2.009	1.877	1.744	1.815
Fe_2	1.333	1.335	1.266	1.383	1.339	1.166	1.184
Mg	0.994	0.89	1.154	0.974	0.833	1.032	1.051
Ca	0.608	0.687	0.58	0.632	0.585	0.525	0.534
Na	0.006	0.001	0	0	0.1	0.095	0.081
K	0	0.001	0	0	0.007	0	0
cationSUM	7.987	7.941	8.007	8.003	8.073	8.134	8.103
Alm	45.421	45.853	42.201	46.258	48.553	42.835	42.755
Py	33.874	30.566	38.46	32.587	30.21	37.89	37.967
Grs	20.705	23.581	19.339	21.155	21.237	19.275	19.278
Fe/Mg	1.34	1.50	1.10	1.42	1.61	1.13	1.13

Epidote			Kyanite	
Rock sample	IV19b_P10_ep_ky	IV 19b C3 P4	Rock sample	IV19b_P19_ky
Mineral	ep	ep	Mineral	ky
SiO_2	38.5	40.25	SiO_2	35.34
TiO_2	0	0.03	TiO_2	0
Al_2O_3	32.62	32.41	Al_2O_3	63.49
Fe_2O_3	1.562	1.545	Fe_2O_3	0
MgO	0	0.04	MgO	0
CaO	25.22	24.01	CaO	0.14
Na_2O	0.3	0	Na_2O	0.49
K_2O	0.03	0	K_2O	0.06
Sum	98.232	98.285	Sum	99.52
Ox	12.5	12.5	Ox	20
Si	2.939	3.043	Si	3.85
Ti	0	0.002	Ti	0
Al	2.934	2.887	Al	8.152
Fe_3	0.09	0.088	Fe_3	0
Mg	0	0.005	Mg	0
Ca	2.062	1.944	Ca	0.016
Na	0.044	0	Na	0.103
K	0.003	0	K	0.008
cationSUM	8.073	7.968	cationSUM	12.13

The multi-stage mechanical reactivation of early fabrics (e.g. S_1) rather than a complete re-building of new fabric at each metamorphic event may be interpreted as due to a highly constrictional strain field imposed by the subduction related mechanics (Andersen et al., 1991; Zulauf, 1997; Zucali et al., 2002a). The constrictional strain field may also be suggested by the relatively stable orientations of the omphacite-, glaucophane-, and garnet-bearing fracture and veins (Fig. 3a), with respect to S_1 and S_2 orientations within Ivozio metabasites and surrounding micaschists (Figs. 2 and 3).

Up to this multiscale structural analysis, lawsonite has generally been interpreted as associated with the retrograde pressure path in the whole Sesia-Lanzo Zone (Pognante et al., 1980; Pognante, 1989b).

Our study shows that the growth of lawsonite in the Ivozio metabasites is prograde, as clearly constrained by meso- and microstructural analysis. Microstructural constraints also demonstrate that the absence of retrograde lawsonite in the described rocks can be consequent to a decompressional retrograde path taking place at a higher temperature than a prograde one (Fig. 8). Moreover, the reconstructed evolution of the Ivozio metabasites contrasts with the metamorphic histories inferred for other lawsonite-bearing localities in the EMC of the Sesia-Lanzo Zone, where lawsonite-bearing assemblages have been described and the growth of lawsonite is ascribed to the retrograde evolution.

In metabasites of EMC of the southern Sesia-Lanzo Zone (in the surroundings of the village of Rocca Canavese), retrograde Alpine lawsonite has been described (Pognante, 1989b, 1991; Spalla and Zulbati, 2003) on the basis of a detailed field and microstructural mapping (Spalla and Zulbati, 2003). This work has been based on the recognition and separation of mesoscopic and microscopic fabric elements, not only on the ground of their orientations and overprinting relations, but also evaluating the metamorphic compatibility of the fabric-marking mineral assemblages, as done for the Ivozio metabasites. Although time-consuming, this approach allows a more complete mesostructural and microstructural evolution to be reconstructed that also relies on the relations between deformation and metamorphism.

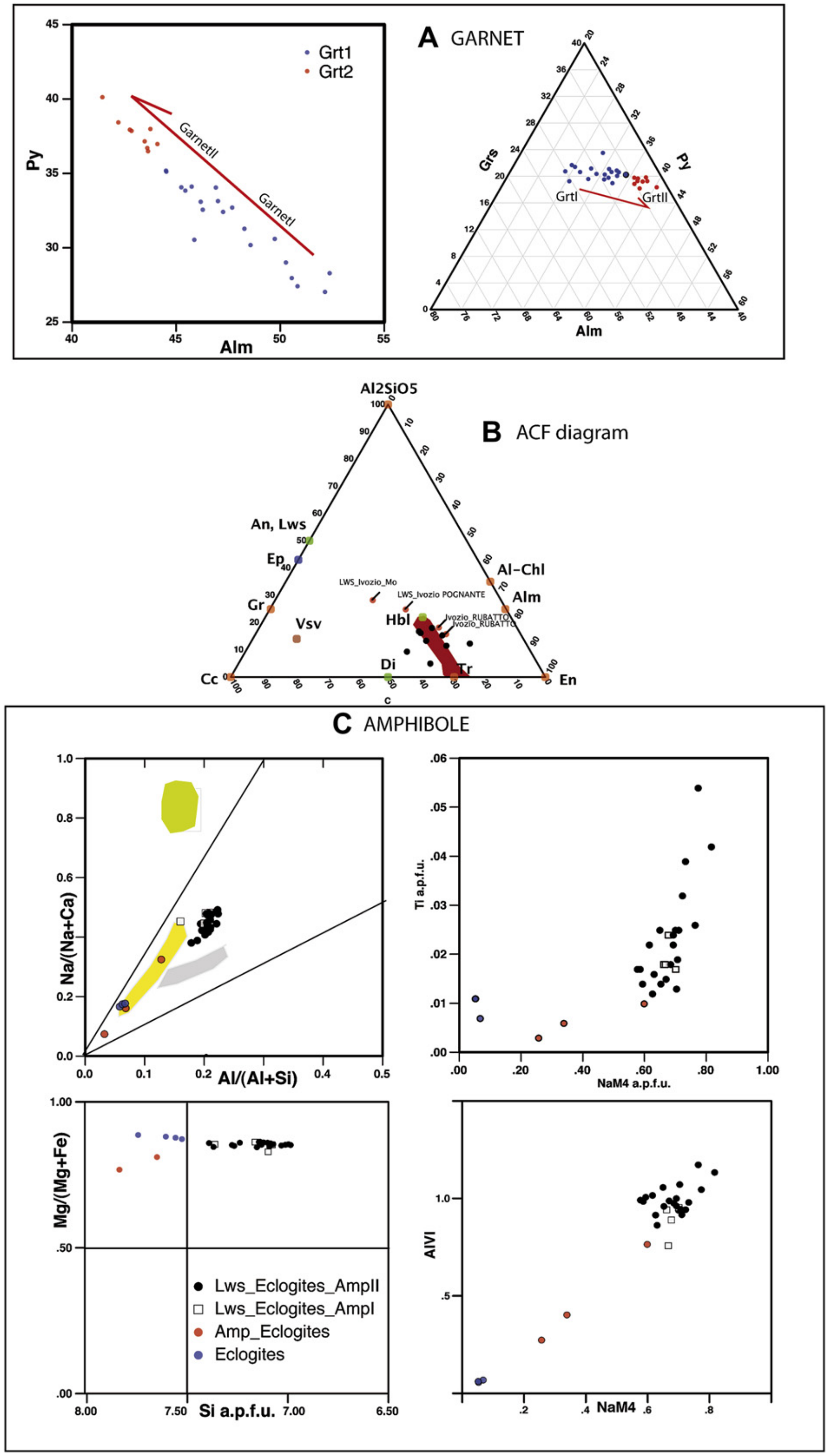

Fig. 7. Mineral chemistry diagrams showing chemical variations with respect to microsites occurrence. A) Garnet compositional variation shown by relative variations of Alm, Py, Grs molecules. B) ACF diagram showing bulk-rock compositional variations among eclogites and lawsonite-bearing eclogites of the Ivozio Complex and other localities of the SLZ (LWS_Ivozio_POGNANTE: Pognante, 1991; LWS_Ivozio_RUBATTO: Rubatto, 1998; LWS_Ivozio_Mo: calculated from molar amount, see Groppo et al., 2009). C) Minerochemical variations of amphibole within lawsonite-bearing eclogites, Amp-eclogites and eclogites. Green, grey and yellow data are after Gosso et al. (2010) from other localities of the SLZ. (For interpretation of the references to colour in this figure legend, the reader is referred to the web version of this article).

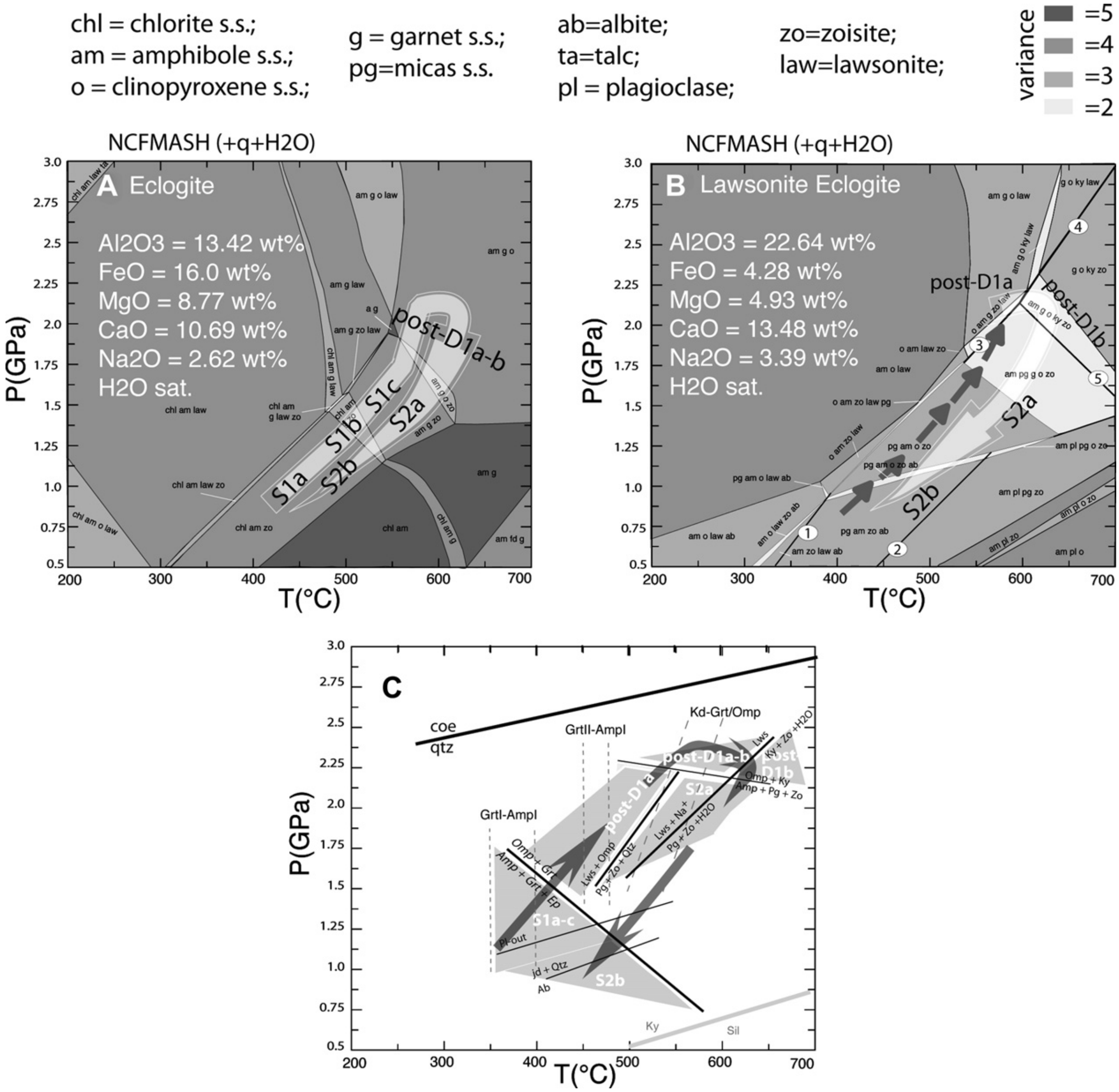

Fig. 8. A and B) Isochemical diagrams (pseudosections) and corresponding P–T–t–d path of the Ivozio Complex metabasites inferred from relative timing of microstructures and metamorphic assemblages superposition (Fig. 5 and Table 1). Grey hatched line in B corresponds to the path inferred from A for stages S_{1a} to S_{1c}. Circled numbers refer to 1) Lws + Ab = Pg + Zo + Qtz + H_2O, 2) transition from Ab end-member to Pl solid solution, 3) Law + Omp = Pg + Zo + Qtz + H_2O, 4) Lws = Zo + Ky + Qtz + H_2O, 5) Omp + Ky = Pg + Am + Zo. C) P–T–t–d path of the Ivozio Complex metabasites inferred using thermobarometrical estimates and experimental equilibria. WmI (Pg) + Ep + Qtz = Lws + Omp, Lws = Zo + Ky + Qtz + H_2O, Lws = Zo + Ky + Qtz + H_2O, Lws + Na^+ = Pg + Zo + H_2O, Omp + Ky = Amp + Pg + Zo reactions (Poli, 1993; Poli and Schmidt, 1995, 1997, 1998; Okamoto and Maruyama, 1999). The reaction of plagioclase disappearance (Pl-out) is after the experiments of Liu et al. (Liu et al., 1996) on the olivine-normative basalt-H_2O system at the amphibolite to eclogite transition. Ky = Sil (Spear, 1993). Equilibria Amp + GrtI + Ep = Omp + GrtII and Ab = Jd + Qtz for eclogites have been recalculated using Thermocalc (Holland and Powell, 1990). Hatched lines show Kd between GrtII and OmpI (Krogh-Ravna and Terry, 2004) and Grt-Hbl calibration of Ravna (2000).

In particular, for the Rocca Canavese metabasites, it is suggested that lawsonite growth is associated with the late stages of development of the S_2 foliation, which overprints the S_1 foliation (Fig. 9). Here, S_1 developed under eclogite-facies conditions and is recorded within relic eclogite boudins that are wrapped by the S_2 foliation. The most pervasive foliation, S_2, is otherwise marked by blueschist facies assemblages, associated with the porphyroblastic growth of lawsonite (Fig. 9).

As mentioned before, lawsonite also occurs in other localities of the Sesia-Lanzo Zone continental crust but for most of these occurrences the relationships between metamorphic mineral growth and the meso- micro-structures are poorly known, suggesting that the retrograde or prograde nature of lawsonite may only be revealed and asserted by the described deformation vs. metamorphism partitioning field-analysis approach.

Fig. 10 compares the constrained P–T–t–d paths of the lawsonite-bearing metabasites from the northern (this work; Zucali et al., 2004) and southern Sesia-Lanzo Zone (Pognante, 1989a), showing the contrasting evolutions followed by two slices belonging to the same metamorphic complex (i.e. EMC). The P–T–t–d path of the northern Sesia-Lanzo Zone (Ivozio Complex), well constrained in this work, is clearly a clockwise path documenting a heating between the P–T peak conditions and the end of the retrograde one, whereas in the southern Sesia-Lanzo Zone,

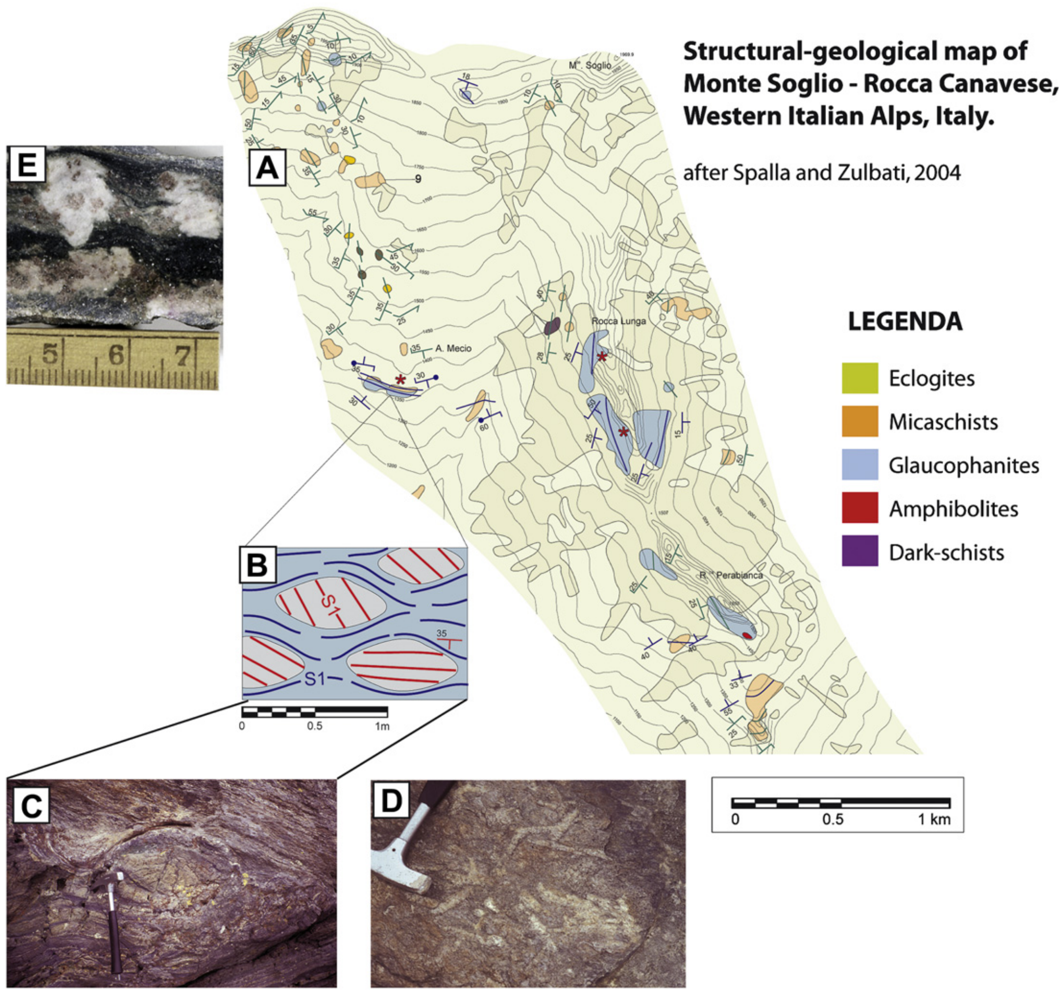

Fig. 9. A) Detail of the structural and petrographic map of the Southern Sesia-Lanzo Zone (Monte Soglio – Rocca Canavese, Western Alps, Italy) (Spalla and Zulbati, 2003). B) Schematic view of the mesoscopic relationships between eclogite boudins, preserving Eclogitic S_1 foliation, wrapped by S_2 blueschists facies lawsonite-bearing foliation. C) Photograph of metre-scale eclogite boudins within lawsonite-bearing glaucophanites (B). D) Lawsonite cm-sized crystals within micaschists. E) Lawsonite cm-sized crystals within glaucophanites. (For interpretation of the references to colour in this figure legend, the reader is referred to the web version of this article).

the retrograde documented evolution, conversely to the northern Sesia-Lanzo Zone, indicates a counterclock-wise path (Pognante, 1989a).

Such peculiar P–T–t–d paths indicate that the EMC consists of at least of two different tectonometamorphic units, even if little is known about the absolute timing of these tectonometamorphic histories. In addition, contrasted P–T evolutions may derive from different paths followed by the single crustal slices within the mantle wedge, developed above the subduction zone (Stockhert and Gerya, 2005; Agard et al., 2009; Meda et al., 2010; Roda et al., 2010) or from the evolution of the thermal gradients characterizing early and mature stages of subduction (e.g. Cloos, 1982). In both cases, these fragments of continental crust were mechanically independent (i.e. decoupled) during their deep burial and exhumation paths and, according to their metamorphic evolution, they coupled together at $P \leq 0.6$ GPa and $T \leq 450$ °C (Pognante, 1989b; Zucali et al., 2004).

These results may be considered within a wider geodynamic setting of the Western Alps and, more in general, of the subduction zone processes. Many mechanisms have been invoked to explain the exhumation of HP or UHP continental rocks such as: slab break-off, slab retreat, crust-mantle delamination, roll-back slab, subduction wedge dynamics (e.g. Chemenda et al., 1995; Ernst et al., 1997; Ring and Layer, 2003; Stockhert and Gerya, 2005; Brun and Faccenna, 2008; Yamato et al., 2008; Meda et al., 2010). Between all these mechanisms only the subduction wedge dynamics can allow the accomplishment of exhumation under highly depressed thermal regimes.

The contrasted P–T evolutions recorded in different portions of the Sesia-Lanzo Zone point to a depressed thermal regime characterizing the exhumation, and, therefore, requires the existence of a mechanism promoting the subduction of crustal slices from the overriding continental plate, before the continental collision as the subduction wedge dynamics.

In addition, the age of 45–37 Ma for the greenschist re-equilibration in the Sesia-Lanzo Zone is within the time span of the eclogitic peak recorded in the meta-ophiolites of Zermatt-Saas, suggesting that exhumation occurred under LP/LT conditions during still active oceanic subduction (e.g. Lapen et al., 2003; Zanoni et al., 2008; Agard et al., 2009).

This set of geological data well fit the predictions from recent numerical modelling of an ocean–continent subduction (Meda et al., 2010; Roda et al., 2010) showing that ablation associated with mantle wedge hydration facilitates both the tectonic sampling and burial of large amount of continental crust from the overriding plate either their exhumation before continental collision.

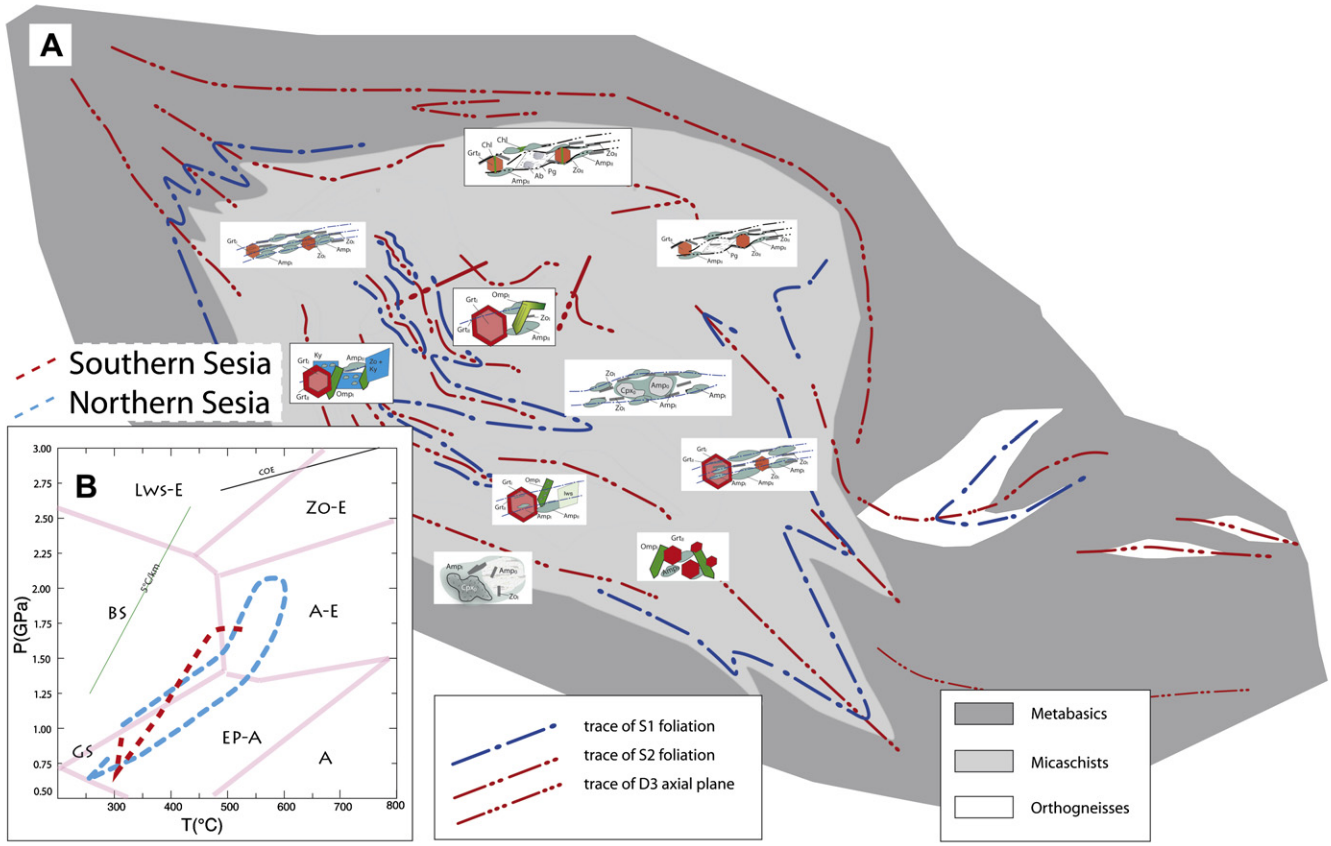

Fig. 10. A) Simplified structural and metamorphic map of the Ivozio metabasites. B) P–T–t–d paths of the Northern (Ivozio metabasites, this work) and Southern Sesia-Lanzo Zone (Pognante, 1989a; Spalla and Zulbati, 2003).

7. Conclusions

This contribution presents a detailed mesostructural and microstructural reconstruction of the Ivozio metabasites' evolution in their burial-exhumation-related path during the Alpine subduction. It shows the complex character of the flow of rocks within a subduction wedge and its relationships with mineral growth.

In detail, this works allows us to reconstruct:

- the development of two main foliations associated with blueschists facies to eclogite-facies metamorphic assemblages, characterized by successive steps of growth and deformation (S_{1a} to post-D_{1b} and S_{2a} to S_{2b}).
- the prograde growth of lawsonite during the post-D_{1a} stage, followed by its replacement by 1) kyanite + zoisite and 2) paragonite pseudomorphs.

The comparison of the P–T–t–d paths of the Ivozio metabasites with lawsonite-bearing rocks from the Sesia-Lanzo Zone shows contrasting tectonometamorphic evolutions. These contrasts suggest that further increase in the detail of the definition of the structural and metamorphic evolutions of similar lawsonite-bearing portions of the EMC, as well as the entire SLZ, is required in order to define the shape and size of those portions that constitute different tectonometamorphic units (Spalla et al., 2005).

The approach used in this contribution, which relates deformational features with the mineral growth at different scales, together with minerochemical evolution of mineral phases, permits us to discriminate between portions of an homogeneous lithostratigraphic unit characterized by contrasting P–T–t–d paths.

The reconstructed Tectonometamorphic Units (TMUs) occurring within a single, lithostratigraphically homogeneous metamorphic complex, are most likely the record of the mechanical processes occurring within the subduction wedge during the ablative-subduction of the overriding continental plate. Such a process facilitates tectonic erosion of small particles that can follow independent paths within the subduction wedge and that may, from time to time, be coupled and decoupled.

Acknowledgements

P.F. Williams is gratefully acknowledged to have imported on the Alps, long ago, a new analytical approach, taking into account the interaction of deformation and metamorphism and their influence on rock memory. Dr. Gisella Rebay and Dr. Manuel Duguet are greatly thanked for their detailed work and important suggestions in the reviews. G. Rebay and C. Groppo are also thanked for helpful suggestions on pseudosection construction. We thank S. Racchetti and F. Zulbati Petrillo that shared with us part of the analytical work and G. Gosso for fruitful discussions. EPMA analyses were carried out with the technical support of A. Risplendente. PRIN 2008 "Tectonic trajectories of subducted lithosphere in the Alpine collisional orogen from structure, metamorphism and lithostratigraphy" fundings are gratefully acknowledged.

References

Agard, P., Yamato, P., Jolivet, L., Burov, E., 2009. Exhumation of oceanic blueschists and eclogites in subduction zones: timing and mechanisms. Earth Science Reviews 92 (1–2), 53–79.

Andersen, T.B., Jamtveit, B., Dewey, J.F., Svensson, E., 1991. Subduction and eduction of continental crust: major mechanisms during continent-continent collision

and orogenic extensional collapse, a model based on the south Norwegian Caledonides. Terra Nova 3 (3), 303–310.
Ballevre, M., Pitra, P., Bohn, M., 2003. Lawsonite growth in the epidote blueschists from the Ile de Groix (Armorican Massif, France); a potential geobarometer. Journal of Metamorphic Geology 21 (7), 723–735.
Bell, T.H., Hayward, N., 1991. Episodic metamorphic reactions during orogenesis: the control of deformation partitioning on reaction sites and reaction duration. Journal of Metamorphic Geology 9, 619–640.
Bell, T.H., Rubenach, M.J., 1983. Sequential porphyroblast growth and crenulation cleavage development during progressive deformation. Tectonophysics 92, 171–194.
Bell, T.H., Rubenach, M.J., Fleming, P.D., 1986. Porphyroblast nucleation, growth and dissolution in regional metamorphic rocks as a function of deformation partitioning during foliation development. Journal of Metamorphic Geology 4, 37–67.
Brun, J.P., Faccenna, C., 2008. Exhumation of high-pressure rocks driven by slab rollback. Earth and Planetary Science Letters 272 (1–2), 1–7.
Caddick, M.J., Thompson, A.B., 2008. Quantifying the tectono-metamorphic evolution of pelitic rocks from a wide range of tectonic settings: mineral compositions in equilibrium. Contributions to Mineralogy and Petrology 156, 177–195.
Caron, J.M., Saliot, P., 1969. Nouveaux gisements de lawsonite et de jadeite dans les Alpes franco-italiennes. (New occurrences of lawsonite and jadeite in the French-Italian Alps). Comptes Rendus Hebdomadaires des Seances de l'Academie des Sciences. Serie D Sciences Naturelles 268 (26), 3153–3156.
Castelli, D., 1991. Eclogitic metamorphism in carbonate rocks; the example of impure marbles from the Sesia-Lanzo Zone, Italian Western Alps. Journal of Metamorphic Geology 9 (1), 61–77.
Cetinkaplan, M., Candan, O., Oberhansli, R., Bousquet, R., 2008. Pressure–temperature evolution of lawsonite eclogite in Sivrihisar; Tavsanli Zone, Turkey. Lithos 104, 12–32.
Chemenda, A.I., Mattauer, M., Malavieille, J., Bokun, A.N., 1995. A mechanism for syn-collisional rock exhumation and associated normal faulting: results from physical modelling. Earth and Planetary Science Letters 132 (1–4), 225–232.
Clarke, G.L., Powell, R., Fitzherbert, J.A., 2006. The lawsonite paradox: a comparison of field evidence and mineral equilibria modelling. Journal of Metamorphic Geology 24 (8), 715–725.
Cloos, M., 1982. Flow melanges: numerical modeling and geologic constraints on their origin in the Franciscan subduction complex, California. Geological Society of America Bulletin 93, 330–345.
Cloos, M., 1993. Lithosferic buoyancy and collisional orogenesis: subduction of oceanic plateaus, continental margins, island arcs, spreading ridges and seamounts. Geological Society of America Bulletin 105, 715–737.
Compagnoni, R., 1977. The Sesia-Lanzo zone: high-pressure low-temperature metamorphism in the Austroalpine continental margin. Rendiconti della Società Italiana di Mineralogia e Petrologia 33, 335–374.
Compagnoni, R., Dal Piaz, G.V., Hunziker, J.C., Gosso, G., Lombardo, B., Wiliams, P.F., 1977. The Sesia-Lanzo Zone: a slice of continental crust, with alpine HP–LT assemblages in the Western Italian Alps. Rendiconti della Società Italiana di Mineralogia e Petrologia 33, 281–334.
Compagnoni, R., Maffeo, B., 1973. Jadeite bearing metagranites l.s. and related rocks in the Mount Mucrone Area (Sesia-Lanzo zone, Western Italian Alps). Schweizerische Mineralogische und Petrographische Mitteilungen 53, 355–378.
Connolly, J., 2005. Computation of phase equilibria by linear programming: a tool for geodynamic modeling and its application to subduction zone decarbonation. Earth and Planetary Science Letters 236, 524–541.
Connolly, J.A.D., 1990. Multivariable phase diagrams; an algorithm based on generalized thermodynamics. American Journal of Science 290 (6), 666–718.
Dal Piaz, G.V., Hunziker, J.C., Martinotti, G., 1972. La Zona Sesia – Lanzo e l'evoluzione tettonico-metamorfica delle Alpi Nordoccidentali interne. Memorie della Società Geoligica Italiana 11, 433–460.
Dale, J., Holland, T., Powell, R., 2000. Hornblende-garnet-plagioclase thermobarometry: a natural assemblage calibration of the thermodynamics of hornblende. Contributions to Mineralogy and Petrology 140, 353–362.
Dale, J., Powell, R., White, R.W., Elmer, F.L., Holland, T.J.B., 2005. A thermodynamic model for Ca–Na clinoamphiboles in Na_2O–CaO–FeO–MgO–Al_2O_3–SiO_2–H_2O–O for petrological calculations. Journal of Metamorphic Geology 23, 771–791.
Ernst, W.G., Maruyama, S., Wallis, S., 1997. Buoyancy driven, rapid exhumation of ultrahigh-pressure metamorphosed continental crust. Proceedings of National Academy of Sciences, U.S.A. 94, 9532–9537.
Furman, M.L., Lindsely, D.H., 1988. Ternary–Feldspar modeling and thermometry. American Mineralogist 73, 201–215.
Gazzola, D., Gosso, G., Pulcrano, E., Spalla, M.I., 2000. Eo-Alpine HP metamorphism in the Permian intrusives from the steep belt of the Central Alps (Languard-Campo nappe and Tonale Series). Geodinamica Acta 13, 149–167.
Gerya, T.V., Stoeckhert, B., Perchuk, A.L., 2002. Exhumation of high-pressure metamorphic rocks in a subduction channel; a numerical simulation. Tectonics 21 (6), 11–19.
Ghent, E.D., Tinkham, D., Marr, R., 2009. Lawsonite eclogites from Pinchi Lake area, British Columbia–new P–T estimates and interpretation. Lithos 109, 248–253.
Gosso, G., 1977. Metamorphic evolution and fold history in the eclogite micaschists of the upper Gressoney valley (Sesia-Lanzo zone, Western Alps). Rendiconti della Società Italiana di Mineralogia e Petrologia 33, 389–407.
Gosso, G., Messiga, B., Rebay, G., Spalla, M.I., 2010. Interplay between deformation and metamorphism during eclogitization of amphibolites in the Sesia–Lanzo Zone of the Western Alps. International Geology Review. doi:10.1080/00206810903529646.
Green, E., Holland, J.G., Powell, R., 2007. An order-disorder model for omphacitic pyroxenes in the system jadeite-diopside-hedenbergite-acmite, with applications to eclogitic rocks. American Mineralogist 92, 1181–1189.
Groppo, C., Forster, M., Lister, G., Compagnoni, R., 2009. Glaucophane schists and associated rocks from Sifnos (Cyclades, Greece): new constraints on the PT evolution from oxidized systems. Lithos 109 (3–4), 254–273.
Hobbs, B.E., Ord, A., Spalla, M.I., Gosso, G., Zucali, M., 2010. The interaction of deformation and metamorphic reactions. In: Advances in Interpretation of Geological Processes: Refinement of Multi-scale Data and Integration in Numerical Modelling. Geological Society of London Special Publication, vol. 332, pp. 189–222.
Holland, T., Baker, J., Powell, R., 1998. Mixing properties and activity-composition relationships of chlorites in the system MgO–FeO–Al_2O_3–SiO_2–H_2O. European Journal of Mineralogy 10, 395–406.
Holland, T.J.B., Powell, R., 1990. An enlarged and updated internally consistent thermodynamic dataset with uncertains and correlations: the system K_2O–Na_2O–CaO–MgO–MnO–FeO–Fe_2O_3–Al_2O_3–TiO_2–SiO_2–C–H_2–O_2. Journal of Metamorphic Geology 8, 89–124.
Holland, T.J.B., Powell, R., 1998. An internally consistent thermodynamic data set for phases of petrological interest. Journal of Metamorphic Geology 16 (3), 309–344.
Koons, P.O., 1982. An Investigation of Experimental and Natural High Pressure Assemblages from the Sesia Zone, Western Alps, Italy. ETH, Zürich.
Kretz, R., 1994. Metamorphic Crystallization. Wiley, 530 pp.
Krogh-Ravna, E., Terry, M.P., 2004. Geothermobarometry of UHP and HP eclogites and schists; an evaluation of equilibria among garnet-clinopyroxene-kyanite-phengite-coesite/quartz. Journal of Metamorphic Geology 22, 579–592.
Lapen, T.J., Johnson, C.M., Baumgartner, L.P., Mahlen, N.J., Beard, B.L., Amato, J.M., 2003. Burial rates during prograde metamorphism of an ultra-high-pressure terrane: an example from Lago di Cignana, Western Alps, Italy. Earth and Planetary Science Letters 215 (1–2), 57–72.
Lardeaux, J.M., Spalla, M.I., 1990. Tectonic significance of P–T–t paths in metamorphic rocks: examples from ancient and modern orogenic belts. Memorie della Società Geoloigica Italiana 45, 51–69.
Lardeaux, J.M., Spalla, M.I., 1991. From granulites to eclogites in the Sesia zone (Italian Western Alps): a record of the opening and closure of the Piedmont ocean. Journal of Metamorphic Geology 9, 35–59.
Li, X.-P., Zheng, Y.-F., Wu, Y.-B., Chen, F., Gong, B., Li, Y.-L., 2004. Low-T eclogite in the Dabie terrane of China: petrological and isotopic constraints on fluid activity and radiometric dating. Contributions to Mineralogy and Petrology 148, 443–470.
Liu, J., Bohlen, S.R., Ernst, W.G., 1996. Stability of hydrous phases in subducting oceanic crust. Earth and Planetary Science Letters 143, 161–171.
Meda, M., Marotta, A.M., Spalla, M.I., 2010. The Role of Mantle Hydration in Continental Crust Recycling in the Wedge Region. Advances in Interpretation of Geological Processes. In: Geological Society, London, Special Publications, pp. 149–171.
Miletto, M., 1984. Struttura e petrografia di un settore del margine esterno della Zona Sesia-Lanzo e del complesso del Monte Cialmera, tra il Monte Cialmera e il Ponte Cusard. Tesi di Laurea, Università di Torino, 179.
Okamoto, K., Maruyama, S., 1999. The high-pressure synthesis of lawsonite in the MORB + H_2O system. American Mineralogist 84 (3), 362–373.
Okay, A.I., 2002. Jadeite-chloritoid-glaucophane-lawsonite schists from northwest Turkey: unusually high P/T ratios in continental crust. Journal of Metamorphic Geology 20, 757–768. doi:10.1046/j.1525-1314.2002.00402.x.
Okay, A.I., Whitney, D.L., 2010. Blueschists, ophiolites, and suture zones in northwest Turkey. Guide-book to the pre-Conference Field Excursion of the GSA meeting: "Tectonic Crossroads: Evolving Orogens of Eurasia-Africa-Arabia 4–8 October 2010 Ankara, Turkey". 54.
Piccarreta, G., 1981. Deep-rooted overthrusting and blueschistic metamorphism in compressive continental margins. An example from Calabria (Southern Italy). Geological Magazine 118, 539–544.
Pognante, U., Talarico, F., Benna, P., 1988. Incomplete blueschist re-crystallization in high-grade metamorphics from the Sesia-Lanzo Unit (Vasario-Sparone Subunit, Western Alps); a case history of metastability. Lithos 21 (2), 129–142.
Pognante, U., 1989a. Lawsonite, blueschist and eclogite formation in the southern Sesia Zone (Western Alps, Italy). European Journal of Mineralogy 1, 89–104.
Pognante, U., 1989b. Tectonic implications of lawsonite formation in the Sesia zone (Western Alps). Tectonophysics 162, 219–227.
Pognante, U., 1991. Petrological constraints on the eclogite- and blueschist-facies metamorphism and P–T–t paths in the Western Alps. Journal of Metamorphic Geology 9, 5–17.
Pognante, U., Compagnoni, R., Gosso, G., 1980. Micro-mesostructural relationships in the continental eclogitic rocks of the Sesia-Lanzo zone: a record of a subduction cycle (Italian Western Alps). Rendiconti della Società Italiana di Mineralogia e Petrologia 36, 169–186.
Pognante, U., Talarico, F., Benna, P., 1987. Incomplete blueschist re-crystallization in high grade metamorphics from the Sesia-Lanzo unit (Vasario – Sparone subunit, Western Alps ophiolites): a case history of metastability. Lithos 21, 129–142.
Poli, S., Schmidt, M.W., 1995. H2O transport and release in subduction zones: experimental constraints on basaltic and andesitic system. Journal of Geophysical Research 100 (B11), 22299–22314.
Poli, S., Schmidt, M.W., 1997. The high-pressure stability of hydrous phases in orogenic belts; an experimental approach on eclogite-forming processes. In: Touret, J.L.R., Austrheim, H. (Eds.), Collisional Orogens; Zones of Active Transfer Between Crust and Mantle. Elsevier, pp. 169–184.

Poli, S., 1993. The amphibolite-eclogite transformation: an experimental study on basalt. American Journal of Science 293, 1061–1107.
Poli, S., Schmidt, M.W., 1998. The high-pressure stability of zoisite and phase relationships of zoisite-bearing assemblages. Contributions to Mineralogy and Petrology 130, 162–175.
Ravna, E.K., 2000. Distribution of Fe^{2+} and Mg between coexisting garnet and hornblende in synthetic and natural systems: an empirical calibration of the garnet-hornblende Fe–Mg geothermometer. Lithos 53 (3–4), 265–277.
Rebay, G., Spalla, M.I., 2001. Emplacement at granulite facies conditions of the Sesia–Lanzo metagabbros: an early record of Permian rifting? Lithos 58 (3–4), 85–104.
Rebay, G., Powell, R., Diener, J., 2010. Calculated phase equilibria for a morb composition in a P-T range, 450-650 °C and 18-28 kbar: the stability of eclogite. Journal of Metamorphic Geology 28, 635–645.
Reddy, S.M., Kelley, S.P., Wheeler, J., 1996. A $^{40Ar/39Ar}$ laser probe study of micas from the Sesia Zone, Italian Alps: implications for metamorphic and deformation histories. Journal of Metamorphic Geology 14, 493–508.
Roda, M., Marotta, A.M., Spalla, M.I., 2010. Numerical simulations of an ocean/continent convergent system: influence of subduction geometry and mantle wedge hydration on crustal recycling. Geochemistry Geophysics Geosystems 11, Q05008. doi:10.1029/2009GC003015.
Ring, U., Layer, P.W., 2003. High-pressure metamorphism in the Aegean, eastern Mediterranean: underplating and exhumation from the Late Cretaceous until the Miocene to recent above the retreating Hellenic subduction zone. Tectonics 22 (3), 1022.
Rubatto, D., 1998. Dating of Pre-Alpine Magmatism, Jurassic Ophiolites and Alpine Subductions in the Western Alps. ETH, Zurich, 174 pp.
Rubatto, D., Gebauer, D., Compagnoni, R., 1999. Dating of eclogite-facies zircons; the age of Alpine metamorphism in the Sesia-Lanzo Zone (Western Alps). Earth and Planetary Science Letters 167 (3–4), 141–158.
Salvi, F., Spalla, M.I., Zucali, M., Gosso, G., 2010. Three-dimensional evaluation of fabric evolution and metamorphic reaction progress in polycyclic and polymetamorphic terrains: a case from the Central Italian Alps. In: Spalla, M.I., Marotta, A.M., Gosso, G. (Eds.), Advances in Interpretation of Geological Processes, 334, pp. 173–187.
Spalla, M.I., Carminati, E., Ceriani, S., Oliva, A., Battaglia, D., 1999. Influence of deformation partitioning and metamorphic re-equilibration on P–T path reconstruction in the pre-Alpine basement of Central Southern Alps (Northern Italy). Journal of Metamorphic Geology 17 (3), 319–336.
Spalla, M.I., Zucali, M., 2004. Deformation vs. metamorphic re-equilibration heteroheneities in polymetamorphic rocks: a key to infer quality P–T–d–t path. Rivista Italiana di Mineralogia e Petrologia 73, 249–257.
Spalla, M.I., Zucali, M., Di Paola, S., Gosso, G., 2005. A critical assesment of the tectono-thermal memory of rocks and definition of the tectonometamorphic units: evidence from fabric and degree of metamorphic transformations. In: Gapais, D., Brun, J.P., Cobbold, P. (Eds.), Deformation Mechanisms, Rheology and Tectonics: From Minerals to the Lithosphere. Geological Society, London, Special Publications, pp. 227–247.
Spalla, M.I., Zulbati, F., 2003. Structural and petrographic map of the southern Sesia-Lanzo Zone; Monte Soglio-Rocca Canavese, Western Alps, Italy. Memorie di Scienze Geologiche 55, 119–127. 1 sheet, 1:10.000 scale.
Spalla, M.I., Siletto, G.B., di Paola, S., Gosso, G., 2000. The role of structural and metamorphic memory in the distinction of tectono-metamorphic units: the basement of the Como lake in the Southern Alps. Journal of Geodynamics 30 (1–2), 191–204.
Spear, F., 1993. Metamorphic phase equilibria and pressure–temperature–time paths. Mineralogical Society of America 799.
Stockhert, B., Gerya, T.V., 2005. Pre-collisional high pressure metamorphism and nappe tectonics at active continental margins: a numerical simulation. Terra Nova 17, 102–110.
Tinkham, D., Ghent, E.D., 2005. Estimating P–T conditions of garnet growth with isochemical phase-diagram sections and the problem of effective bulk-composition. The Canadian Mineralogist 43, 35–50.
Tropper, P., Essene, E.J., 2002. Thermobarometry in eclogites with multiple stages of mineral growth: an example from the Sesia-Lanzo Zone (Western Alps, Italy). Schweizerische Mineralogische und Petrographische Mitteilungen 82, 487–514.
Tropper, P., Essene, E.J., Sharp, Z.D., Hunziker, J.C., 1999. Application of K-feldspar-jadeite-quartz barometry to eclogite facies metagranites and metapelites in the Sesia Lanzo Zone (Western Alps, Italy. Journal of Metamorphic Geology 17 (2), 195–209.
Tsujimori, T., Sisson, V.B., Liou, J.G., Harlow, G.E., Sorensen, S.S., 2006. Very-low-temperature record of the subduction process: a review of worldwide lawsonite eclogites. Lithos 92, 609–624.
Yamato, P., Burov, E., Agard, P., Le Pourhiet, L., Jolivet, L., 2008. HP–UHP exhumation during slow continental subduction: Self-consistent thermodynamically and thermomechanically coupled model with application to the Western Alps. Earth and Planetary Science Letters 271 (1–4), 63–74.
Zanoni, D., Bado, L., Spalla, M.I., Zucali, M., Gosso, G., 2008. Structural analysis of the northeastern margin of the tertiary intrusive stock of Biella (Western Alps, Italy). Bollettino della Società Geologica Italiana (Italian Journal of Geosciences). 127 (1), 125–140.
Zucali, M., 2009. jPT – mineral formula calculation and geo-thermobarometry. http://users.unimi.it/mzucali/dev/java/JPTproject/.
Zucali, M., Chateigner, D., Dugnani, M., Lutterotti, L., Ouladdiaf, B., 2002a. Quantitative texture analysis of naturally deformed hornblendite under eclogite facies conditions (Sesia-Lanzo Zone, Western Alps): comparison between X-ray and neutron diffraction analysis. In: De Meer, S., Drury, M.R., De Bresser, J.H.P., Pennock, G.M. (Eds.), Deformation Mechanisms, Rheology and Tectonics: Current Status and Future Perspectives, vol. 200, pp. 239–253.
Zucali, M., Spalla, M.I., Gosso, G., 2002b. Strain partitioning and fabric evolution As A correlation tool: the example of the eclogitic micaschists complex in the Sesia-Lanzo Zone (Monte Mucrone – Monte Mars, Western Alps Italy). Schweizerische Mineralogische und Petrographische Mitteilungen 82, 429–454.
Zucali, M., Spalla, M.I., Gosso, G., Racchetti, S., Zulbati, F., 2004. Prograde LWS-KY transition during subduction of the Alpine continental crust of the Sesia-Lanzo Zone: the Ivozio Complex. In: Evolution of the Western Alps: Insights from Metamorphism, Structural Geology, Tectonics and Geochronology. Journal of Virtual Explorer 16 paper 4.
Zulauf, G., 1997. Constriction due to subduction: evidence for slab pull in the Mariánské Lázně complex (central European Variscides). Terra Nova 9 (5–6), 232–236.